

---

# LOW-COST SPACE STRUCTURE (LCSS) EXPERIMENT

Volume I of II

David DeYoung  
Lawrence Robertson, III

SVS R&D Systems Inc.  
6207 Pan American Freeway NE  
Albuquerque, NM 87109

June 1996

Final Report

Distribution authorized to DoD components only; Proprietary Information; June 1996. Other requests for this document shall be referred to AFMC/STL.

**WARNING** - This document contains technical data whose export is restricted by the Arms Export Control Act (Title 22, U.S.C., Sec 2751 et seq.) or The Export Administration Act of 1979, as amended (Title 50, U.S.C., App. 2401, et seq.). Violations of these export laws are subject to severe criminal penalties. Disseminate IAW the provisions of DoD Directive 5230.25 and AFI 61-204.

**DESTRUCTION NOTICE** - For classified documents, follow the procedures in DoD 5200.22-M, Industrial Security Manual, Section II-19 or DoD 5200.1-R, Information Security Program Regulation, Chapter IX. For unclassified, limited documents, destroy by any method that will prevent disclosure of contents or reconstruction of the document.

19961009 098

DTIC QUALITY INSPECTED 2



**PHILLIPS LABORATORY**  
Space and Missiles Technology Directorate  
AIR FORCE MATERIEL COMMAND  
KIRTLAND AIR FORCE BASE, NM 87117-5776

---

UNCLASSIFIED



AD NUMBER

AD-B214 765

NEW LIMITATION CHANGE

TO

DISTRIBUTION STATEMENT A -  
Approved for public release; Distri-  
bution unlimited.

Limitation Code: 1

FROM

DISTRIBUTION STATEMENT -

Limitation Code:

AUTHORITY

Janet E. Mosher; Phillips Lab/CA, Kirtland AFB,  
N.M.

THIS PAGE IS UNCLASSIFIED

# DISCLAIMER NOTICE



**THIS DOCUMENT IS BEST QUALITY AVAILABLE. THE COPY FURNISHED TO DTIC CONTAINED A SIGNIFICANT NUMBER OF PAGES WHICH DO NOT REPRODUCE LEGIBLY.**

Using Government drawings, specifications, or other data included in this document for any purpose other than Government procurement does not in any way obligate the U.S. Government. The fact that the Government formulated or supplied the drawings, specifications, or other data, does not license the holder or any other person or corporation; or convey any rights or permission to manufacture, use, or sell any patented invention that may relate to them.

This report contains proprietary information and shall not be either released outside the government, or used, duplicated or disclosed in whole or in part for manufacture or procurement, without the written permission of the contractor. This legend shall be marked on any reproduction hereof in whole or in part.

If you change your address, wish to be removed from this mailing list, or your organization no longer employs the addressee, please notify PL/VTS, 3550 Aberdeen Ave SE, Kirtland AFB, NM 87117-5776.

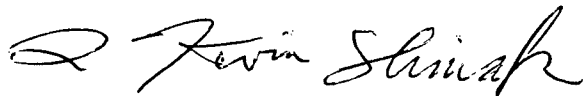
Do not return copies of this report unless contractual obligations or notice on a specific document requires its return.

This report has been approved for publication.



RICHARD COBB, Capt, USAF  
Project Manager

FOR THE COMMANDER



L. KEVIN SLIMAK, GM-15  
Chief, Structures and Controls Division



CHRISTINE M. ANDERSON, SES, DAF  
Director, Space and Missiles Technology  
Directorate

The following notice applies to any unclassified (including originally classified and now declassified) technical reports released to "qualified U.S. contractors" under the provisions of DoD Directive 5230.25, Withholding of Unclassified Technical Data From Public Disclosure.

NOTICE TO ACCOMPANY THE DISSEMINATION OF EXPORT-CONTROLLED TECHNICAL DATA

1. Export of information contained herein, which includes, in some circumstances, release to foreign nationals within the United States, without first obtaining approval or license from the Department of State for items controlled by the International Traffic in Arms Regulations (ITAR), or the Department of Commerce for items controlled by the Export Administration Regulations (EAR), may constitute a violation of law.
2. Under 22 U.S.C. 2778 the penalty for unlawful export of items or information controlled under the ITAR is up to two years imprisonment, or a fine of \$100,000, or both. Under 50 U.S.C., Appendix 2410, the penalty for unlawful export of items or information controlled under the EAR is a fine of up to \$1,000,000, or five times the value of the exports, whichever is greater; or for an individual, imprisonment of up to 10 years, or a fine of up to \$250,000, or both.
3. In accordance with your certification that establishes you as a "qualified U.S. Contractor", unauthorized dissemination of this information is prohibited and may result in disqualification as a qualified U.S. contractor, and may be considered in determining your eligibility for future contracts with the Department of Defense.
4. The U.S. Government assumes no liability for direct patent infringement, or contributory patent infringement or misuse of technical data.
5. The U.S. Government does not warrant the adequacy, accuracy, currency, or completeness of the technical data.
6. The U.S. Government assumes no liability for loss, damage, or injury resulting from manufacture or use for any purpose of any product, article, system, or material involving reliance upon any or all technical data furnished in response to the request for technical data.
7. If the technical data furnished by the Government will be used for commercial manufacturing or other profit potential, a license for such use may be necessary. Any payments made in support of the request for data do not include or involve any license rights.
8. A copy of this notice shall be provided with any partial or complete reproduction of these data that are provided to qualified U.S. contractors.

D E S T R U C T I O N      N O T I C E

For classified documents, follow the procedures in DoD 5200.22-M, Industrial Security Manual, Section II-19 or DoD 5200.1-R, Information Security Program Regulation, Chapter IX. For unclassified, limited documents, destroy by any method that will prevent disclosure of contents or reconstruction of the document.

# DRAFT SF 298

<b>1. Report Date (dd-mm-yy)</b> June 1996		<b>2. Report Type</b> Final		<b>3. Dates covered (from... to )</b> 04/95 to 06/96	
<b>4. Title &amp; subtitle</b> Low-Cost Space Structure (LCSS) Experiment , Volume I			<b>5a. Contract or Grant #</b> F29601-93-C-0205		
			<b>5b. Program Element #</b> 62601F		
<b>6. Author(s)</b> David DeYoung Lawrence Robertson, III			<b>5c. Project #</b> 3005		
			<b>5d. Task #</b> C0		
			<b>5e. Work Unit #</b> DL		
<b>7. Performing Organization Name &amp; Address</b> SVS R&D Systems Inc. 6207 Pan American Freeway NE Albuquerque, NM 87109				<b>8. Performing Organization Report #</b>	
<b>9. Sponsoring/Monitoring Agency Name &amp; Address</b> Phillips Laboratory 3550 Aberdeen Ave SE Kirtland AFB, NM 87117-5776				<b>10. Monitor Acronym</b>	
				<b>11. Monitor Report #</b> PL-TR-96-1059 Vol I of II	
<b>12. Distribution/Availability Statement</b> Distribution authorized to DoD components only; Proprietary Information: June 1996. Other requests for this document shall be referred to AFMC/STI					
<b>13. Supplementary Notes</b>					
<b>14. Abstract</b> The Low-Cost Space Structure (LCSS) experiment was a two-year Phase II Small Business Innovative Research (SBIR) technology program to develop the concept for a small, lightweight, space-borne optical imaging system. The goals of the program were to formulate the concept design of a sparse array optical imaging system and the supporting satellite and to validate the concept in a laboratory demonstration. The results are described in this final report. They show that a high-resolution imaging system based on this concept can be fielded in space at a small fraction of the cost of systems with similar capabilities. The laboratory effort demonstrated high precision and medium bandwidth closed-loop control for the tilt and piston simultaneously. Commercial spin-off applications were identified for the track processor developed for the breadboard experiments.					
<b>15. Subject Terms</b> Space imaging, space structures, sparse apertures, optical controls					
<b>Security Classification of</b>			<b>19. Limitation of Abstract</b>	<b>20. # of Pages</b>	<b>21. Responsible Person (Name and Telephone #)</b>
<b>16. Report unclassified</b>	<b>17. Abstract unclassified</b>	<b>18. This Page unclassified</b>	Limited	54	Capt Richard Cobb (505) 846-8255

**SBIR Rights Notice**

These SBIR data are furnished with SBIR rights under USAF/PL Contract No. F29601-93-C-0205. For a period of four (4) years after acceptance of all items to be delivered under this contract, the Government agrees to use these data for all Government purposes only, and they shall not be disclosed outside the Government (including disclosure for procurement purposes) during such period without permission of the Contractor, except that, subject to the foregoing use and disclosure prohibitions, such data may be disclosed for use by support Contractors. After the aforesaid four (4) year period, the Government has a royalty free license to use, and to authorize others to use on its behalf, these data for Government purposes, but it is relieved of all disclosure prohibitions and assumes no liability for unauthorized use of these data by third parties. This notice shall be affixed to any reproductions of this data, in whole or in part.

## TABLE OF CONTENTS

Section	Page
LIST OF FIGURES.....	vi
LIST OF TABLES.....	vii
LIST OF ACRONYMS.....	viii
1.0 INTRODUCTION.....	1
2.0 DEFINITIONS.....	1
3.0 SUMMARY RESULTS.....	1
4.0 BACKGROUND.....	2
5.0 CONCEPT DESIGN.....	3
5.1 PAYLOAD.....	4
5.1.1 Payload Optical Control System Description and Phasing of the Optical System.....	4
5.1.2 Phasing of the Optical System.....	4
5.1.3 Payload Component Description.....	6
5.1.4 Mechanical Design.....	6
5.1.5 Electrical Power Requirement.....	9
5.1.6 Payload Computer Subsystem.....	9
5.1.6.1 Hardware Design.....	9
5.1.6.2 Software Design.....	10
5.1.6.2.1 Payload Computer Initialization.....	10
5.1.6.2.2 Payload Computer Operation.....	10
5.1.7 Telemetry and Data Storage.....	12
5.1.8 Thermal Control.....	13
5.2 SPACECRAFT.....	13
5.2.1 Structural and Mechanical.....	13
5.2.2 Electrical Power System (EPS).....	15
5.2.2.1 EPS Requirements.....	16
5.2.2.2 EPS Description.....	16
5.2.3 Stabilization and Attitude Control (SAC) Subsystem.....	17
5.2.4 Flight Computer.....	19
5.2.5 Telemetry.....	19



5.2.6 Thermal Control System (TCS).....20

5.2.7 System Characterization and Tuning Unit (SCTU).....20

6.0 PERFORMANCE MEASURES.....20

6.1 SPACECRAFT PERFORMANCE .....20

6.1.1 Flexible Control Performance.....22

6.1.2 Attitude Control Performance .....24

6.2 PAYLOAD PERFORMANCE.....25

6.2.1 Objectives/Error Budget.....25

6.2.2 Point-Spread Function (PSF).....25

6.2.3 Subaperture Phasing Error Budget.....26

6.2.4 Signal-to-Noise Ratio (SNR) and Line-of-Sight (LOS) Stability  
Allocation.....27

6.2.5 Acquisition Error Budgets .....27

6.2.5.1 Acquisition Camera Acquisition Error Budget .....27

6.2.5.2 Optical Bench Acquisition Error Budget.....27

6.2.6 Radiometric Sensitivities.....28

6.3 SATELLITE MASS PROPERTIES.....29

6.4 ORBITAL PERFORMANCE .....29

6.5 MASS EXPULSION SYSTEM MARGINS .....29

7.0 LABORATORY EXPERIMENT.....30

7.1 EXPERIMENT BREADBOARD DESCRIPTION.....30

7.1.1 Breadboard Optical Design.....30

7.1.2 Sensor Descriptions.....31

7.1.3 Steering Mirrors.....31

7.1.4 Computer Systems .....32

7.1.5 Boom .....34

7.2 CONTROL LOOPS .....35

7.2.1 Operation Sequence .....35

7.2.2 Tilt Control.....36

7.2.3 Fine Piston Control.....37

7.3 TEST RESULTS.....38

7.3.1 Disturbance Environment .....38

7.3.2 Pseudo-aperture Test Results.....39

7.3.3 Full System Test Results.....39

7.3.4 Translation Sensing.....40

7.3.4.1 Error Budget Validation .....41

7.3.4.2 Translation Measurement Accuracy.....41

8.0 CONCLUSIONS .....42

## LIST OF FIGURES

Figure		Page
5.1.1-1	The optical control architecture.....	5
5.1.4-1	Required component spacing.....	8
5.2.1-1	Main plate design.....	14
5.2.1-2	Ring frames, stringers, and end plates.....	15
5.2.2.2-1	Hierarchical “and” tree of the EPS.....	17
5.2.3-1	Top-level SAC signal flow diagram.....	18
6.1-1	Spacecraft pointing error budget for payload target acquisition.....	21
6.1-2	Spacecraft pointing stability budget for payload target acquisition.....	22
6.1-3	Acquisition camera error budget.....	22
6.1.1-1	LCSS flex dynamics simulation.....	23
6.1.2-1	SIMULINK groundsite simulation.....	25
6.2.1-1	Optical alignment error budget.....	26
6.2.2-1	LCSS data - system PSF.....	26
6.2.5.2-1	Optical bench acquisition error budget.....	28
6.2.6-1	Radiometric sensitivities of the LCSS two-aperture system.....	28
7.1.1-1	Breadboard experiment optical layout.....	30
7.1.4-1	Tree breakdown of software.....	33
7.1.5-1	Picture of the boom apparatus (not to scale).....	35
7.2.2-1	LCSS tilt loop setup.....	36
7.2.3-1	Piston sensing algorithm.....	38

## LIST OF TABLES

<b>Table</b>	<b>Page</b>
5.1.2-1 Payload control loops.....	7
5.1.3-1 Table of payload elements.....	8
5.1.5-1 Payload component power requirements.....	9
5.1.6.2.2-1 Summary chart of the LCSS software modes.....	11
5.2.1-1 Satellite structure mass.....	13
5.2.2.1-1 EPS calculated requirements.....	16
5.2.4-1 Planned usage percentages and goals for the flight computer.....	19
6.1.1-1 LOS Error from simulation.....	24
6.3-1 Subsystem breakdown of the satellite mass.....	29
6.4-1 Decay time vs. altitude.....	29
7.1.2-1 Sensor parameters.....	31
7.1.5-1 General boom characteristics.....	34
7.3.1-1 Disturbance environment.....	39
7.3.2-1 Pseudo aperture test results of the lab experiment.....	40
7.3.3-1 Full system test results of the lab experiment.....	40
7.3.4.1-1 Error budget verification of the fringes per meter resolution with a result of 0.55 wave per micron.....	41
7.3.4.2-1 Resolution capability results for primary mirror #1.....	42
7.3.4.2-2 The rms Values of Opti-Track tracking error.....	42

**LIST OF ACRONYMS**

ACQ	Acquisition Card
A/D	Analog to Digital
ATP	Acquisition, Tracking, and Pointing
BMU	Battery Management Unit
BRT	Beam Reduction Telescope
BSM	Beam Steering Mirror
CPU	Central Processing Unit
DDB	Design DataBook
DOD	Depth of Discharge
DOF	Degree of Freedom
EOL	End of Life
EPS	Electrical Power System
FOV	Field of View
GSE	Ground Support Equipment
IMOS	Integrated Modeling of Optical Systems
I/O	Input/Output
LCSS	Low Cost Space Structures (refers to the LCSS experiment)
LEC	Lateral Effects Cell
LED	Light Emitting Diode
LOS	Line-of-Sight
NASA	National Aeronautics and Space Administration
OPD	Optical Path Difference
PDU	Power Distribution Unit
PSD	Power Spectral Density
PSF	Point Spread Function
RMS	Root Mean Square
RPV	Remote Pilotless Vehicle
RSC	Remote Signal Conditioner
SAC	Stabilization and Attitude Control
SBIR	Small Business Innovative Research
SCTU	System Characterization and Tuning Unit
SDIO	Strategic Defense Initiative Office
SNR	Signal-to-Noise Ratio
SPU	Solar Power Unit
SRD	System Requirements Document
TBD	To Be Determined
TCS	Thermal Control System
USAF	United States Air Force

## 1.0 INTRODUCTION

This purpose of this report is to summarize SVS's Phase II efforts on the Low-Cost Space Structure (LCSS) Small Business Innovative Research (SBIR) project. The main thrust of this phase was to further develop the LCSS system to the "concept design" stage and perform a risk reduction laboratory breadboard experiment of a scaled version of the LCSS payload. The main results of the risk reduction laboratory breadboard experiment, a summary of the system concept, a commercialization effort overview, and a project summary are all included in this report.

Throughout this report, several large, SVS-generated documents will be referenced. These documents were all deliverables to the customer and included the Design DataBook (DDB), which contains the full laboratory breadboard experiment report, and the System Requirements Document (SRD). This report summarizes the results of these two documents and provides a general overview of the project.

## 2.0 DEFINITIONS

Throughout this report, several terms will be used that are defined as follows:

- **Launch Vehicle**     the vehicle or carrier used to place the satellite into orbit (or if appropriate, into suborbit)
- **Spacecraft**         (sometimes called the bus) the structure and associated equipment used to house and maintain the payload so that it can perform its mission
- **Payload**             the (optical) experiment and its subsystems
- **Satellite**            the combination of the spacecraft and the payload
- **GSE**                  pre-mission and real-time ground support equipment (GSE)

## 3.0 SUMMARY RESULTS

The Phase II LCSS SBIR project was initiated to further develop the LCSS system concept of a low-cost, small-package-size, space-based, sparse-aperture imaging satellite. The focus of the project was directed toward four specific areas: developing the system concept, performing risk reduction experiments, developing preliminary designs of certain high-risk components and, although not a primary task but an important SBIR goal, commercialization of the concept. All of the above major tasks were completed according to the Phase II LCSS contract.

Documentation of the Phase II effort culminated in the development of the LCSS DDB and SRD. The DDB concept was created by the LCSS's Chief Engineer, Dr. Sherman Seltzer, to act like a "skunkworks" type of blueprint. The LCSS DDB "blueprint" contains all of the design information about the project and is complete in its description of the system concept. Any additions or changes to the LCSS design were contingent on the approval of the Chief Engineer.

The SRD, similar in concept to the DDB, compiles all of the project requirements into one place with changes or addition as per approval of the Chief Engineer. These two documents serve as the mainstay documents for any SVS project and contain all of the project design information. These documents have been used continuously on this project and will continue to be used.

Specific to the LCSS project, the DDB provides a complete systems concept of everything from the payload system to the spacecraft design to the spacecraft/launch vehicle interface system. In addition, certain risk reduction designs of the payload main plate and spacecraft/launch vehicle structure were included in the DDB.

Also included in the DDB are the results of the laboratory breadboard experiment. This experiment was designed to show the feasibility of the LCSS optical payload and to demonstrate the ability to phase the two segments of the sparse primary and common secondary telescope. A 1/4-scale design of the flight telescope and full-scale equivalent of the phasing control system were built for the laboratory test. A boom dynamically similar to the flight boom was also incorporated into the breadboard experiment. The main results of the experiment were that the tilt loops could be controlled at the required 100-Hz tilt loop error and the piston loop algorithms were successful to the point that a piston control loop was implemented with a high degree of control.

Another major milestone of the project was the successful commercialization effort of the LCSS concept. Preliminary conversations with Rockwell International have been fruitful at jointly selling the LCSS concept to a national surveillance organization. NASA also showed interest in the LCSS concept and their requirements will be addressed in the near future.

In addition to the main commercialization effort, a number of LCSS spin-off technologies are at various stages of commercialization. These spin-off technologies include the commercially successful tracking software-hardware system Opti-Trak and the power line inspection system INSPECT. All of these projects have paying commercial customers.

#### **4.0 BACKGROUND**

The present LCSS pointing concept grew from a concept development in a Phase I SBIR contract between Dr. Sherman M. Seltzer and the Innovative Research Office of the Strategic Defense Initiative Office (SDIO). It involved developing a space experiment concept that optically and dynamically emulates a large optical space system. The experiment was constrained to be inexpensive, lightweight, and simple. It also must perform in a realistic space environment, i.e. "zero-g" and no atmosphere. The approach investigated whether significant elements of acquisition, tracking, and pointing (ATP) can be demonstrated for a particular set of spaceborne optical telescope programs. This would be achieved with an experiment composed of a few representative critical sparse optical elements. These elements would be incorporated into a small satellite to be launched from a space shuttle as a Hitchhiker payload. The use of sparse elements will minimize the cost, weight, and size of the experiment, while the Hitchhiker approach substantially reduces the launch costs.

Specifically, during Phase I, the feasibility was investigated to accurately emulate a large space optical telescope consisting of a spatially correct sparse optical payload on-board a small satellite. After orbital insertion, stowed sparse components would be deployed to the correct distances with representative structural dynamics. They represent a spacecraft-borne large optical telescope that can be pointed and controlled with the desired accuracy. The experiment is not designed to investigate the full breadth of structural dynamics problems. It will, however, demonstrate the accurate precision pointing and control of any given class of large military optical systems in space. It is only in space that one can obtain a realistic test of precision pointing and control of structural dynamics.

As a result of the successful Phase I, Dr. Seltzer joined with SVS Inc. and together submitted a winning Phase II SBIR proposal to the USAF Phillips Laboratory. Because of the significant commercialization potential found during Phase I, the objectives for the Phase II were modified and broadened from those originally envisioned at the beginning of Phase I.

The new goal of the proposed effort was to capitalize on an initially unexpected major breakthrough achieved in Phase I. This breakthrough is the development of a versatile self-contained optical payload system package. Specifically, the Phase II goal was to complete the concept design of the self-contained optical payload package so that, in Phase III, it could be manufactured as a "black box" with appendages. For example, a proprietary highly accurate sparse-aperture concept has been developed that can be applied to a number of missions. The self-contained optical system can be mounted onboard any desired carrier, such as an orbiting satellite (as originally envisioned), an aircraft, a remote pilotless vehicle (RPV), or a balloon.

The LCSS concept definition will be demonstrated by developing (in follow-on phases), manufacturing and operating (in Phase III) a sparse-aperture experiment that will adequately demonstrate in space a powerful and low-cost means of verifying precision pointing and control of a broad class of space optical telescopes. It is proposed to use the satellite that was developed in Phase I, although other carriers could be used. The results of this experiment will provide future program managers with a means of verifying necessary pointing and control performance in aerospace before actually embarking on costly programs. Because performance in space is often quite different from the predicted or tested ground results, an important void will be filled by implementing the proposed LCSS pointing concept.

## 5.0 CONCEPT DESIGN

The concept design can be broken down into two pieces: the spacecraft and the payload. Together they constitute the satellite. The spacecraft and the payload are, in turn, composed of a number of subsystems including:

### *Payload*

- Optical Control System
- Mechanical
- Electrical Power



- Computer
- Data Storage
- Interfaces

### *Bus or Spacecraft*

- Structure and Mechanical
- Electrical Power System
- Stabilization and Attitude Control System
- Flight Computer
- Telemetry
- Thermal Control System
- System Characterization Unit

## **5.1 PAYLOAD**

The function requirements of the payload are to control tilt, translation, and piston of primary mirror segments such that phasing can be accomplished. The payload was designed to be capable of imaging stars, satellites, and perform earth surveillance.

### **5.1.1 Payload Optical Control System Description and Phasing of the Optical System**

Figure 5.1.1-1 depicts the optical/control architecture design and was used as the blueprint for the breadboard experiment design. This control architecture performs alignment of the optical path of the two primary segments by utilizing low-frequency coarse control of the segments themselves and high-frequency control of the line-of-sight (LOS) of the segments by utilizing fast steering mirrors on the optical bench. The optical system is corrected such that the science camera can observe distant objects such as stars, satellites and earth objects with a large effective aperture. Initial acquisition of the target object is accomplished using the acquisition camera and the satellite control system.

### **5.1.2 Phasing of the Optical System**

Once the target object is in the acquisition camera's field of view (FOV), phasing of the optical elements is carried out to properly image the target object. The optical system is phased by controlling tilt, translation, and piston of the optical system. By using two primary segments, the optical path of one segment is used as a reference, and the other optical path is controlled to the reference.

Translation control of the primary segments is performed by moving the primary segments with motorized stages. One light emitting diode (LED) is attached to each primary segment at the edge. The LEDs are imaged onto the translation camera. The primary segments are translated such that the images of the LEDs are aligned to empirically determine optimum locations on the translation camera.

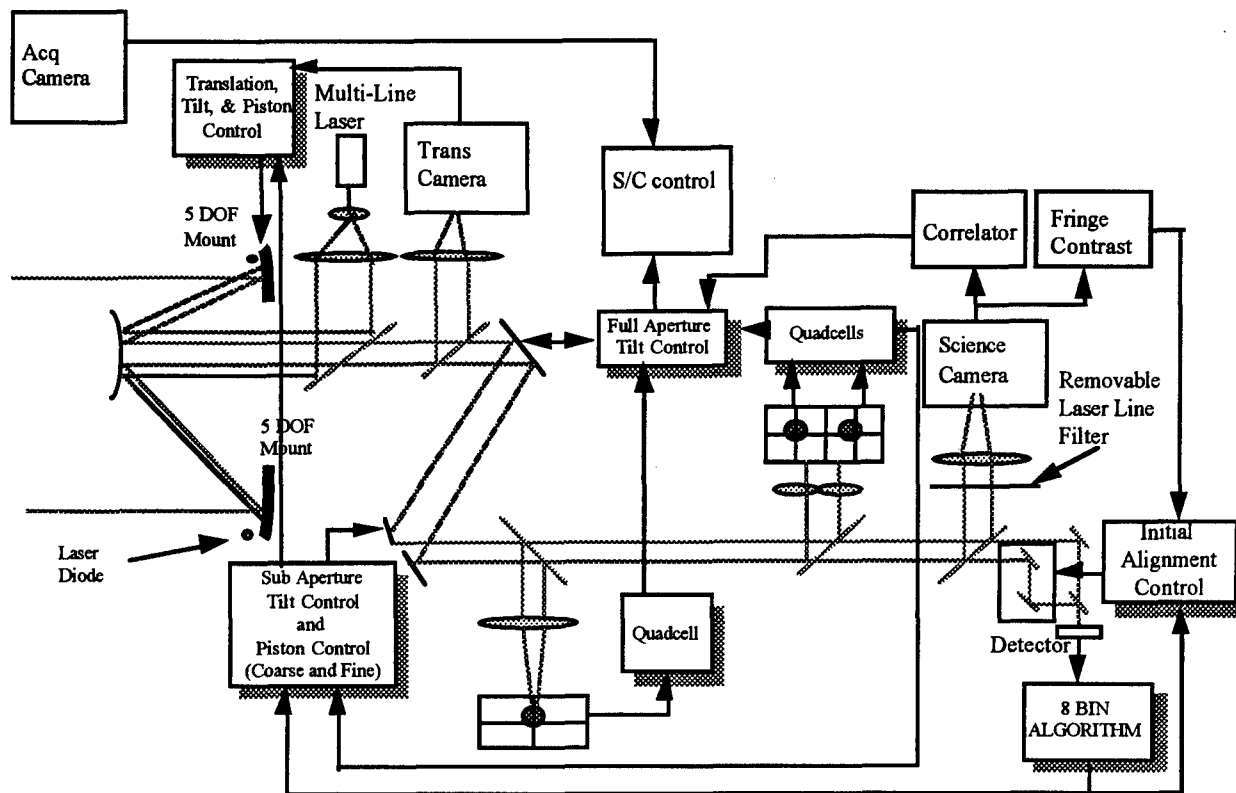


Figure 5.1.1-1. The optical control architecture.

Once the translation control has been optimized, the translation stages freeze, holding their last commanded position. By utilizing the shallow depth-of-field properties of the translation camera, translation control of the primary segments along the optical axis (z-axis) of the system was controlled by finding the optimum focus location of the images of the LEDs on the translation camera. Once the optimum focus for each primary segment was found, the z-axis control of each segment was also set to freeze, holding their last commanded position.

At this point, the LEDs are turned off, the on-board laser is turned on, and the translation camera lens system is set for infinity focus. With the lens system in this position, the laser return from the primary segments imaged onto the translation camera represents the tilt of the primary segments. Using empirically determined optimum locations for the laser intensity onto the translation camera, coarse tilt control of the primary segments can be achieved. This 2-axis-per-segment tilt control can either be set to freeze holding last commanded position or can run in closed-loop control, depending on the disturbance environment of the particular engagement.

Acquiring the spot with subaperture tilt sensor one is the next step in phasing the system. Using BSM #1 as the control actuator, close the track loop to center the spot. Next, acquire the second spot using subaperture tilt sensor number two. Close a track loop around subaperture tilt sensor number two and BSM #2. These two tilt loops both have 100-Hz open-loop crossovers.

The next step is to acquire with the piston sensor and perform piston alignment between the science camera and piston sensor. Signal intensity on the piston sensor is appropriately verified. Both beams are now overlapped on this sensor. To acquire the piston error signal, scan the coarse piston mirror drive to find peak intensity output of the piston detector. Hold (i.e. freeze) the coarse piston mirror at this position. The optical path difference (OPD) between beam 1 and 2 is now within 1/2 wave. Once 1/2-wave-error is achieved, fine-track piston control can be entered. Fine-track control is done using the piston dither, 8-bin algorithm. Remove laser line-blocking filter from the science camera. Scan the initial alignment control and simultaneously compute fringe contrast of science camera. While the initial alignment control is scanning, the fine-track piston control off-loads to coarse drive. Once peak fringe contrast is found on the science camera, the initial alignment control is set for hold/cage position. The piston sensor and science camera are now piston aligned. The laser line-blocking filter is now reinserted in front of the science camera. Table 5.1.2-1 details the control loops utilized on the LCSS payload.

### 5.1.3 Payload Component Description

Along with defining the control architecture and phasing methodology, the payload component specifications were completed as part of the LCSS system concept. Each component was defined using the particular subsystem performance requirements defined for that part of the optical control architecture. Table 5.1.3-1 lists each of the payload components designed, the particular optical control subsystem where the component resides, and the section of the DDB where the component specification can be found.

### 5.1.4 Mechanical Design

A mechanical layout has been completed for the payload optical system discussed in Section 5.1.3. Figure 5.1.4-1 details the required component spacings. This design conforms to the allotted payload main plate diameter. The design was implemented by utilizing two levels. The entrance element to the payload bench optical system is the 8.7x beam reduction telescope. The upper optical bench contains the mount for the 8.7x beam reduction telescope, the low-power laser, which is used as the phasing source, and the science camera. The lower payload optics bench contains the remainder of the payload optical components. Components included on the lower optics platform are: both beam steering mirrors, the translation camera, the intermediate tilt sensor, the subaperture tilt sensor, the piston sensor, and the 5x beam reduction telescope.

Table 5.1.2-1. Payload control loops.

Loop	Sensor	Source	BW (Hz)	Control Objective	Movable Element
Acquisition Tilt	Acquisition Camera 30 Hz	Star - 1 Spot	0.1	Hold Spot at Fiducial	Satellite Attitude
Intermediate Tilt	Quad Cell	Star - 1 Spot	10	Hold spot at fiducial	BSM1 with off-load to satellite
Fine Tilt	Quad Cell	Multiline Laser - 1 Blob (1/segment)	100	Hold blob at fiducial	BSM1 with off-load to satellite
Subaperture Tilt	Quad Cell	Multiline laser - 2 spots (1/segment)	100	Hold spots at fixed offset w.r.t. each other	BSM2 (tilts optical path of 1 segment only) with off-load to segment tilt
Segment Tilt	Translation Camera 30 Hz	Multiline Laser - 2 spots (1/segment)	0.1	Tilt segments to achieve correct separation between 2 spots	Segment 5 - DOF mount
Segment Translation	Translation Camera 30 Hz	2 LEDs 1/segment	0.1/ Open	Translation segments w.r.t. each other	Segment 5 - DOF mount
Segment Focus	Translation Camera 30 Hz	2 LEDs 1/segment	0.1/ Open	Piston segments to sharpen focus	Segment 5 - DOF mount
Piston Acquisition/ Coarse	Piston Sensor	Multiline Laser	0.1	Drive coarse piston translator to peak fringe on piston sensor	Coarse piston translator
Initial Alignment Control	Science Camera and Piston Sensor	Multiline Laser	0.1/ Open	Align piston sensor to science camera	Initial alignment translator, BSM1 piston, coarse piston
Scene Correlation	Science Camera 60 Hz	Earth object	3	Full frame correlation on object of interest	BSM1 with off-load to satellite
Piston/Fine	Piston Sensor LEC	Multiline Laser	3	Piston 1 segment w.r.t. other to increase sharpness	BSM2 (pistons optical path of 1 segment only)

Table 5.1.3-1. Table of payload elements.

Component Name	Optical Control Subsystem	DDB Section
Acquisition Camera	Acquisition Control	4.3.1.1
LEC for Intermediate Tilt Control	Intermediate Tilt Control	4.3.2.1
Beam Steering Mirror (BSM) #1	Intermediate Tilt Control and Subaperture Tilt Control	4.3.2.2
LEC for Fine Tilt Control	Subaperture Tilt Control	4.3.3.1
Multiline Laser	Subaperture Tilt Control and Fine Piston Control	4.3.3.3 & 4.3.11
LEC for Subaperture Tilt Control	Subaperture Tilt Control	4.3.4.1
Beam Steering Mirror (BSM) #2	Subaperture Tilt Control and Fine Piston Control	4.3.4.2 & 4.3.11
Translation Camera	Segment Tilt Control	4.3.5.1
5-Degree of Freedom (DOF) Mirror Mounts	Segment Tilt Control and Segment Focus	4.3.5.2 & 4.3.7
Translation Camera Beam Splitter	Segment Tilt Control	4.3.5.3
Telescope Segment Light Emitting Diodes (LED)	Segment Translation and Segment Focus	4.3.6.1 & 4.3.7
Translation Camera	Segment Translation and Segment Focus	4.3.6.2 & 4.3.7
Translation Stages	Segment Translation	4.3.6.3
Piston Sensor	Piston Sensor Acquisition and Course Control and Fine Piston Control	4.3.8.1 & 4.3.11
Course Piston Translator	Piston Sensor Acquisition and Course Control	4.3.8.2
Initial Alignment Control Translator	Initial Alignment Control	4.3.9.1
Science Camera Fringe Contrast and Tilt Control	Initial Alignment Control	4.3.9.2 & 4.3.9.3
Correlation Tracker	Initial Alignment Control	4.3.9.4
Telescope Segment Optics	Telescope Segment Optics	4.3.12

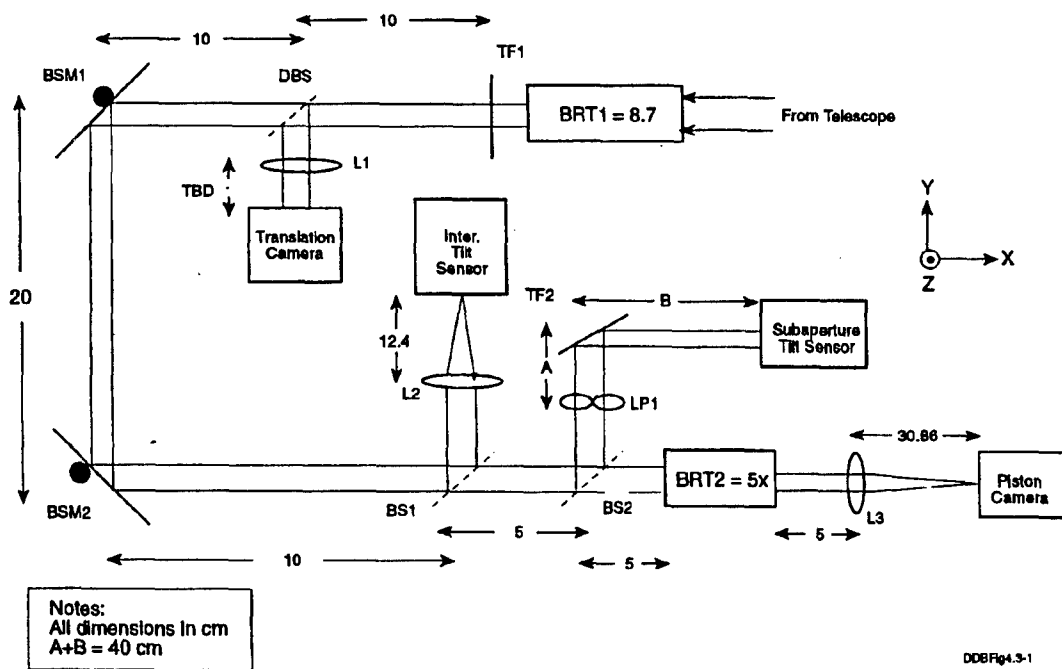


Figure 5.1.4-1. Required component spacing (picture not to scale).

### 5.1.5 Electrical Power Requirement

The power allocated for the payload components is listed in Table 5.1.5-1.

Table 5.1.5-1. Payload component power requirements.

Payload Component Name	Power Per Components (Watts)	Total Power (Watts)
Multiline Laser	5	5
Computer	30	30
Cameras (Translation, Science)	4	8
BSM #1	30	30
BSM #2	30	30
LEDs (2)	1	2
Piston Course Track Translator	10	10
Silicon Position Sensitive Devices (3)	4	12
Silicon Detector (Piston Sensor)	4	4
Science Camera Filter Positioner	10	10
5-DOF Stages (2)	50	100
Data Recorder	27	27
<b>TOTAL PAYLOAD POWER</b>		<b>268</b>

### 5.1.6 Payload Computer Subsystem

This section gives the layout of the hardware and software description for the payload computer system. A complete computer software and hardware description can be found in the LCSS Computer Software Mode Logic Section and Section 4.6 of the DDB.

#### 5.1.6.1 Hardware Design

The computer will have 16 analog input channels and will perform calculations, control system digital compensation, mode decision making, and output signals by 24 channels of analog output to the payload's steerable optics. Image processing from the payload cameras will be accomplished in the track processor contained in the payload computer. Image processing results are also output via the analog output channels. The computer system will be a single backplane buss-type system. The computer must be capable of performing digital control-loop compensation for the 24 channels of analog output at 2000 Hz. All of these calculations must be completed in double precision floating point arithmetic. Digital logic level outputs (discrete) should also be provided by the payload processor for controlling the modes of any payload components that require them (tape recorders, cameras, mirror controllers, etc.). The payload computer must also provide the interface and software to record all payload data on the tape recorder. RS 422 and MIL-STD 1553 busses will connect the payload computer to the spacecraft computer. The analog input channels should have programmable gain, offset, and filtering control to ease sensor integration and allow reprogrammability for system tuning. The system must be capable of sampling all 16 channels at a minimum sample rate of 2000 Hz (20 times higher than fastest control loop).

The analog output channels should be capable of adjusting the output value at the minimum rate of 2000 Hz on all 24 channels. Each channel should provide for fast output settling at 10 microseconds nominal.

### 5.1.6.2 Software Design

Software for the computer system was designed to handle the control commands for the payload system. The architecture was designed to check and initialize all of the flight computer hardware, initialize all of the payload hardware and provide commands to the payload systems during operations. This section is only concerned with the payload software and does not take into account any of the bus computer software.

#### 5.1.6.2.1 Payload Computer Initialization

Upon power-on, the CPU loads the kernel from ROM and then runs the start-up script. The start-up script spawns the *lcssExec* task.

The *lcssExec* task is the top-level executive process in the LCSS computer. It has the responsibility for managing all subtasks in the processor and handling errors and commands to the other processes.

The *lcssExec* task operates the payload computer through initialization operations (commanding and status) and shutdown.

During initialization, the *lcssExec* task verifies the existence of the other computer hardware components. First, it attempts to initialize the analog-to-digital converter. If a buss error results, the task sets an error state and proceeds. Second, the task attempts to initialize the digital-to-analog converter board. If this results in a buss error, the task sets an error state and continues. Third, the task attempts to initialize the tracker hardware. If an error results, the *lcssExec* task accumulates all errors notifies the operator, and exits. If all initializations complete successfully, the *lcssExec* process spawns the analog-to-digital conversion task *adStart()*. This task is an infinite loop that reads the analog input registers and converts the values read to volts and places them into global memory locations. After spawning the *adStart* task, the *lcssExec* task spawns the digital-to-analog conversion task *daStart()*. This task is an infinite loop which reads global memory locations and outputs the voltage values stored there on the analog channels. Then the *lcssExec* task spawns the tracker executive task *rvtExec()*. After spawning these tasks, the *lcssExec* task enters a command and status loop where it executes operator commands, monitors and reports system status, and sequences through experiment modes.

#### 5.1.6.2.2 Payload Computer Operation

After the computer system has been initialized, the *lcssExec* routine will be responsible for implementing an experiment mode logic sequence. This sequence can be implemented using a script control language such as Tcl. The experiment script will be capable of determining current

experiment status and, based on the current state and status decides the logical next step and commands the *lcssExec* routine to transition the payload computer to that state.

Payload computer modes reflect the experimental control modes on a one-for-one basis as much as possible. Certain experimental control modes require additional modes in the payload processor and track processor. In these cases, modes have been added with a letter appended to the respective control mode. The computer modes are listed as follows in Table 5.1.6.2.2-1. A more detailed explanation of the computer software modes can be found in Section 4.6.2.2 of the DDB.

The majority of mode sequencing requires the tracker process to alter states, thus the *lcssExec* process will pass commands to the *rvtExec* process which will adjust the tracker variables according to the desired state. Tracker outputs will be routed to the proper control loop and actuator channel by the *lcssExec* task. In some cases the *rvtExec* process may execute a specific tracker task for a given experiment mode.

Table 5.1.6.2.2-1. Summary chart of the LCSS software modes.

Mode	Function	Data	Pass	Fail
0	BSM calibration	LEC #1 detector output	Transformation matrix for calibration of BSM #1 actuator commands to tilt commands calculated	Software notifies user and exits
1a	Translation Camera Initial Acquisition (Detection)	Tracker output for detection	Successful diode detection	Adjust threshold, adjust gain size, scan mirror
1b	Translation Camera Initial Acquisition (Acquisition)	Tracker output for acquisition	Successful diode acquisition	Adjust threshold, adjust gain size, scan mirror
2	Translation Camera Acquisition Sequencing	Tracker multiple target outputs	Acquisition of targets in each of the five track gains	Reposition mirror, check diodes
3	Translation Camera Translation Track	Multiple track gate positions	Centroid of each set of diodes in same position, geometry of each set of diodes the same	Adjust mirror positions, check for diode acquisition
4	Translation Camera Tilt Track	Multiple track gain positions	Geometry and position of track and sets matching	Adjust mirror tilt, check for x and y alignment, check diode acquisition
5	Translation Camera Focus Track	Track gate spot size	Smallest track spot sizes	Reaccomplish translation tilt track



Table 5.1.6.2.2-1. Concluded.

6a	Acquisition Camera Object Acquisition (Detection)	Tracker detection data	Acquisition of target	Adjust threshold, adjust track gate size, scan for target
6b	Acquisition Camera Object Acquisition (Acquisition)	Tracker acquisition data	Acquisition of target	Adjust threshold, adjust track gate size, scan for target
7	Acquisition Camera Control	Acquisition camera target track error	Place target within 1/4 intermediate camera's FOV of center of acquisition camera	Reaquire target in acquisition camera
8	Intermediate Sensor Acquisition	LEC error signals	Centering of beam on LEC using BSM #1	TBD
9	Intermediate Sensor Track	LEC error, compensation calculation	Target placed to within 40 microrad of center of intermediate FOV	Reaquire in the intermediate sensor
10	Subaperture Tilt Sensor #1 Acquisition	Intensity output of sensor	Target on the sensor	Scan mirror, increase performance of intermediate track
11	Subaperture Tilt Sensor #1 Track	LEC outputs	Target in center of LEC	Reaquire target in LEC, increase performance of the high-bandwidth control loop
12	Subaperture Tilt Sensor #2 Acquisition	LEC intensity output	Target on sensor	Better subaperture #1 tracking, require
13	Subaperture Tilt Sensor #2 Track	LEC outputs	Target of center of LEC	Reaquire on subaperture #2 better control loop performance
14a	Piston Sensor Acquisition (Detection)	Piston sensor output, tracker output	Detection of target	Better tracking on the subaperture #2 sensor
14b	Piston Sensor Acquisition (Acquisition)	Piston sensor output, tracker output	Acquisition of target	Detection, subaperture #2 tracking
15	Piston Sensor Track	Piston Sensor tracker output	Tracking of target to center of the piston sensor	Reacquisition on piston sensor, improved performance on the 5- DOF control loop

### 5.1.7 Telemetry and Data Storage

For the LCSS design, the telemetry requirement was calculated to be approximately 1015 kbits per second with a total number of 3.26E+08 bits of data stored during a typical 5-minute mission

scenario. The Odetics model 3100 tape recorder was identified as a representative payload telemetry data recorder that could meet the requirements. A more complete breakdown of the telemetry requirements and characteristics of the Odetics model 310 can be found in DDB Sections 4.7 and 4.8 respectively.

### 5.1.8 Thermal Control

Thermal control requirements of the payload system were identified and outlined in Section 4.9 of the DDB. The thermal control apparatus was identified in the bus section of the DDB.

## 5.2 SPACECRAFT

The function requirements of the spacecraft is to provide attitude control, stabilization, power, thermal, and structural support of the payload. Each of these subsystems was designed to support a mission lifetime of six months.

### 5.2.1 Structural and Mechanical

The satellite structure must provide for mounting all the spacecraft subsystems and for attachment and deployment from the flight carrier. For many spacecraft, the structure can be very lightweight with stiffness and frequency requirements driven only by the launch vehicle and upper stage boost loads and environments. However, this small satellite must meet these type requirements plus stiffness and frequency requirements driven by the on-orbit experiments to be performed.

The satellite structure must be lightweight to avoid a high overhead penalty; thus, the design approach was to simplify the satellite structure such that the equipment mounting, carrier attachment and deploy loads are supported in one plate. In addition, since one main plate is used, it also serves as the optical bench for the payload.

Table 5.2.1-1. Satellite structure mass.

Part	Mass (kg)
Main Bench	29.50
Solar Array Support Structure	2.27
Deployable Booms	13.60
Optics Cover	9.07
Payload Computer Structure	6.80
<b>TOTAL</b>	<b>61.20</b>

The satellite structure contains five major elements. These are:

- the main plate; used as the optical bench for the payload and at the bottom of the satellite
- the optics cover

- the spacecraft computer structure
- ring frames, stringers, and end plates
- the deployable boom

Calculated estimates of the structural mass are shown in Table 5.2.1-1. Figure 5.2.1-1 shows the design of the main plate. Figure 5.2.1-2 shows a picture of the ring frames, stringers and end plates.

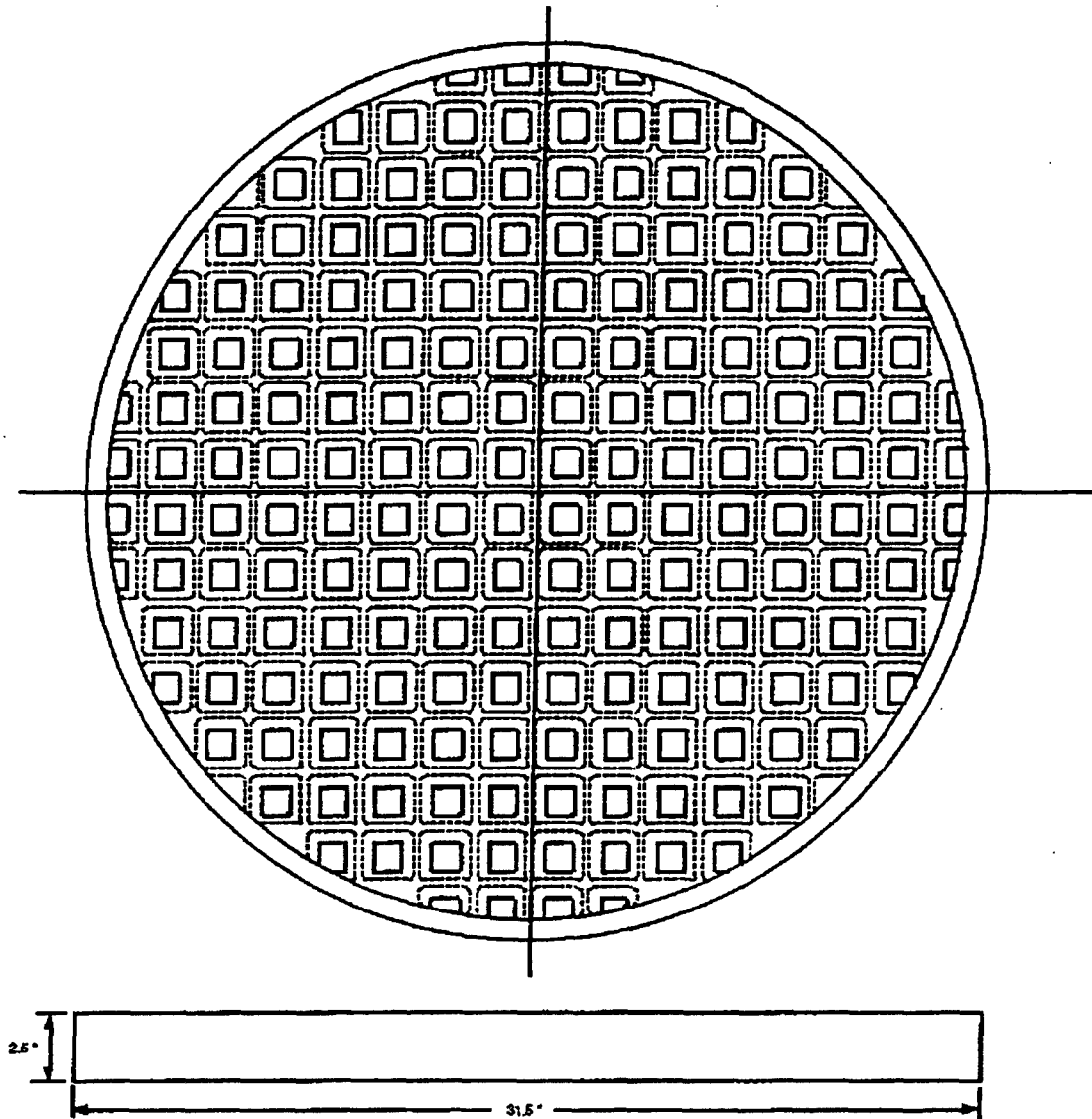


Figure 5.2.1-1. Main plate design.

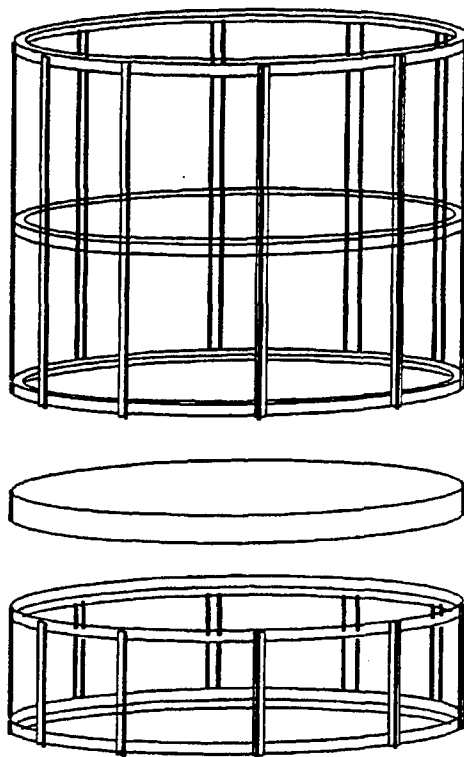


Figure 5.2.1-2. Ring frames, stringers, and end plates.

### 5.2.2 Electrical Power System (EPS)

The following sections describe an approach to EPS design based on the use of optional loads to control bus overvoltage. The Phase I design used a sequential shunt unit to control bus overvoltage. Each design approach has advantages and disadvantages, mainly related to thermal load management, thus, the next design phase should model each approach, assess the trade-offs and decide on the proper approach

During the designing of the EPS several assumptions were made to simplify the analysis. These assumptions are as follows:

1. Power requirements identified in the Phase I effort for the various loads are essentially unchanged.
2. Battery redundancy assumption from Phase I effort is extended to include the solar array, Battery Management Unit (BMU), and the Power Distribution Unit (PDU).
3. The requirement for the development of various voltage levels other than unregulated 28 Vdc or regulated 28 Vdc is removed from the PDU and assigned to the various loads.
4. Experiment duration is 10 minutes maximum.
5. The payload will have a separate power bus.

- 6. Maximum solar array temperature will not exceed 42°C and minimum solar array temperature will not be less than -55°C.
- 7. A 22-cell battery will be used.

**5.2.2.1 EPS Requirements**

The power requirements for the LCSS system are shown in Table 5.2.2.1-1. This table is a condensed versions of the more complete DDB tables found in Section 5.2.2. Included in the DDB power discussions are a more complete breakdown of the power requirements and how they effect the total power. A complete discussion of the assumptions used can also be found in the DDB.

Table 5.2.2.1-1. EPS calculated requirements.

	Base Load	Day Load	Night Load	Exp Delta P	Optional
<b>Total Load Power (W)</b>	112.78	112.18	114.18	123.30	351.82
<b>Payload Bus Load Power (W)</b>	25.00	25.00	25.00	93.40	93.40
<b>Battery Bus Load Power (W)</b>	22.24	22.24	22.24	0.00	210.80
<b>Main Bus Load Power (W)</b>	65.54	64.94	66.94	29.90	47.62
<b>Total Average EPS Power (W)</b>	146.69	144.82	148.37	148.29	378.68

Sizing of the solar arrays was also completed as part of the Phase II effort. After taking into account a worst-case sun incidence angle, an end-of-life (EOF) degradation factor, the power needed and other factors, a total number of 20 parallel solar cells strings are required to supply the current necessary to achieve the Total Average EPS Power (i.e. for the day) and at the same time recharge the batteries which supplied the Total Average EPS Power (i.e. for the maximum length night with a 10 minute experiment and a recharge fraction of 1.06). A more complete discussion can be found in DDB Section 5.2.3.

Battery capacity of the LCSS system was determined for a 25% and 50% depth of discharge (DOD). A total battery capacity was calculated using a degrading factor of 0.825 of the nameplate cell capacity. For a two-battery EPS the required battery nameplate capacity ranged between approximately 4 A-hr. (i.e., 8.06/2) and 10 A-hr. (i.e., 19.54/2).

**5.2.2.2 EPS Description**

For the Phase II effort a description of the EPS bus system was completed. A hierarchical “and” tree of the EPS system is shown in Figure 5.2.2.2-1. Engineering drawings of the EPS system can

be found in Section 5.2.5 of the DDB. A guide to the EPS operations was also devised as part of the Phase II effort and can be found in Section 5.2.6 of the DDB.

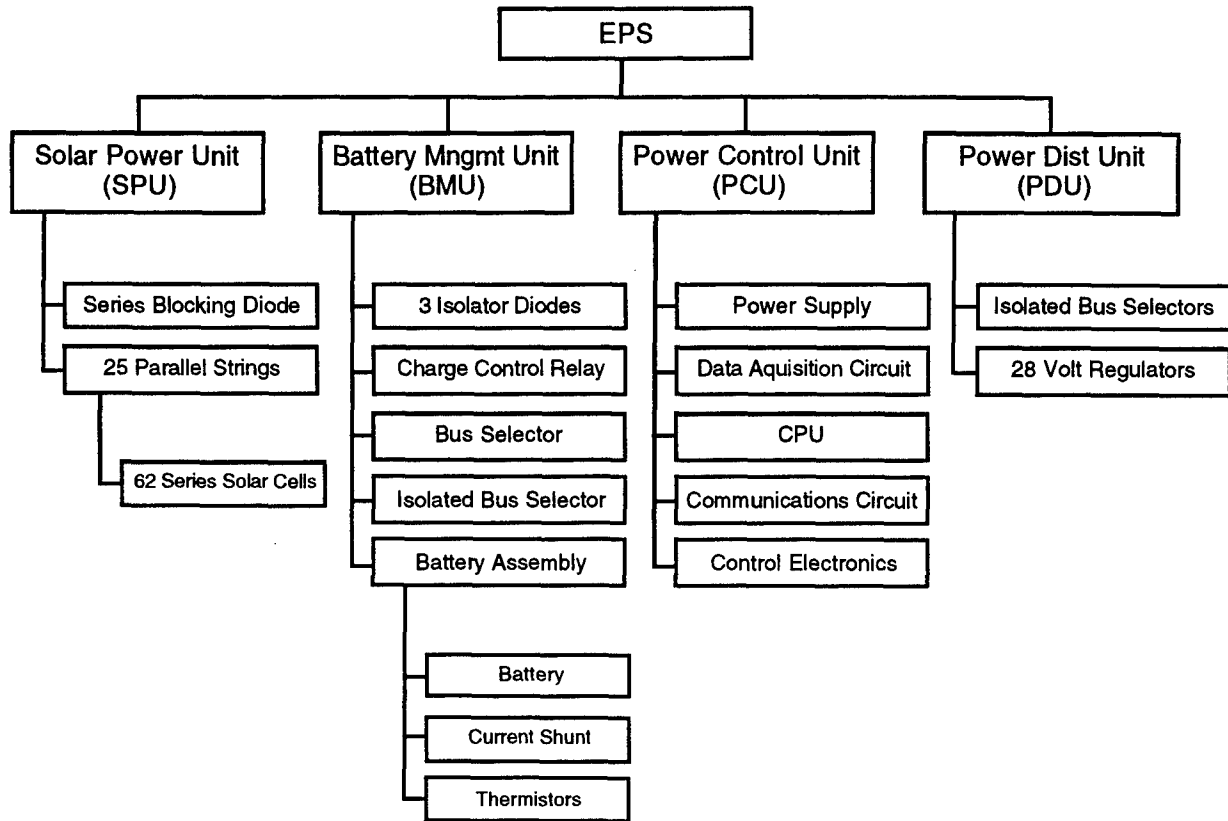


Figure 5.2.2.2-1. Hierarchical "and" tree of the EPS.

**5.2.3 Stabilization and Attitude Control (SAC) Subsystem**

The design approach for the SAC subsystem was to use devices that minimize resource usage yet serve dual purposes. In the pitch axis, the reaction wheels were combined with horizon scanners into "Scanwheels®". The magnetic torque rods which control the attitude during non-experiment periods also serve a dual purpose since the reaction wheels and scanwheels must have a source for dumping momentum. The torque rods also serve a backup role as a tumble recovery system. Another design approach incorporated was the use of a two-level attitude measuring system. The coarse attitude is constantly measured using a three-axis magnetometer, while the fine attitude needed for experiment runs is determined by a more precise set of instruments, thus the fine-attitude sensors can be powered down when not in use to conserve energy. For high-rate experiment maneuvers, the reaction control system is augmented with a cold gas thruster system about the pitch axis. The cold gas supply may also be used to augment the System Characterization and Tuning Unit.

The attitude control system contains the following major elements:

- Pitch axis horizon scanwheels (2)
- Roll axis and yaw axis reaction wheels
- Magnetic torque rods for each axis
- Three-axis magnetometer
- Actuator drive electronics
- 4-p steradian sun sensor set
- Cold gas thruster system for pitch axis
- Inertial attitude reference unit
- Global Positioning Sensor (GPS) receiver
- Flight computer GNC/ACS software

The block diagram shown in Figure 5.2.3-1 illustrates the top-level signal flow of the attitude control system.

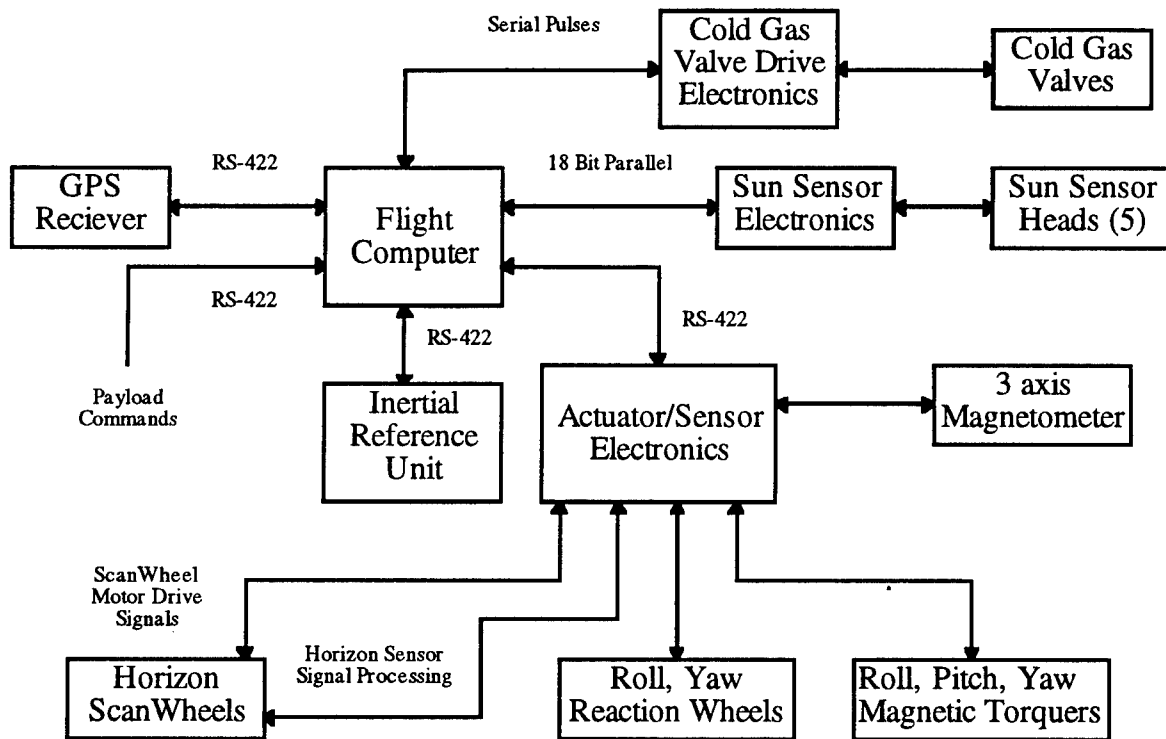


Figure 5.2.3-1. Top-level SAC signal flow diagram.

Also developed during the Phase II effort were the SAC operation logic. Developed were both a nominal pointing operation and a four-mode experiment pointing operation. SAC performance during the nominal mode was approximated to have an attitude error of 2.5 degrees.

#### 5.2.4. Flight Computer

The design approach for the flight computer was to use an existing space-qualified system that has flight history, plenty of developed interface boards, and a software development support system with adequate documentation. The baselined choice for the flight computer was the Honeywell S-5. The S-5 can satisfy all of the requirements stated in Table 5.2.4-1. The definition of the software tasks and the planned usage requirements are TBD, but using the loaded goals in Table 5.2.4-1, the characteristics of the flight computer can be determined as per Table 5.2.4-1.

Table 5.2.4-1. Planned usage percentages and goals for the flight computer.

<b>Flight Computer Characteristic</b>	<b>Parameter</b>
CPU Capability	10 MIPS per CPU
Max Memory Usage	256k local, 512k global per CPU
I/O Throughput	1.0 Mbits/s all channels summed
CPU Usage	50%
Planned Memory Usage	75%
Rated I/O Throughput Usage	25%

The flight computer will contain the following major elements: two central processing unit (CPU) boards with local memory, one board with shared global memory, two I/O boards and one utility board, internal and external restart capability. The baselined choice for the flight computer was the Honeywell S-5. The S-5 can satisfy all of the requirements stated above. It is radiation-hard to 50k rad total dose, therefore it is usable for a short-duration,

#### 5.2.5 Telemetry

The design approach for the telemetry system was to minimize complexity by eliminating redundancy in the primary system. A secondary low-rate back-up system will provide the necessary redundancy. This was considered acceptable by using off-the-shelf, flight-proven, vendor components as much as possible. Another design consideration was to use some of the new, small, low-power components. However, the newer technology must still have a flight performance record in order to be considered with this type of approach.

The primary telemetry system contains the following major elements: PCM encoder, S-Band FM transmitter with > 1 MHz bandwidth, S-Band power amp, 15 watt or 28 watt output (optional), S-Band FM receiver with > 256 kHz bandwidth, S-Band low-noise receiver pre-amp with NF<1 dB, G=15 dB (optional), uplink data decoder, diplexer, right-hand circular polar hemispherical antenna, telemetry I/O controller, telemetry recorder, and RF switches. Additional elements will be added if the uplink and/or downlink telemetry must be encrypted. The equipment chosen can be interfaced to either the KG-66 or KGV-68. A set of radio link margins and downlink and uplink operations for the LCSS telemetry system were also developed.



### 5.2.6 Thermal Control System (TCS)

The design approach for the TCS was simplified by the fact that the main plate (optical bench) will act as a large thermal conductor and thermal capacitance to even out the operating temperature of the elements mounted on the bench (most elements are mounted directly to the bench or piggy-backed directly onto other structures such that heat conductance will have a path to the optical bench). Dedicated deployable radiators will be attached to the rim of the main plate. In addition the large booms deployed for the experiment will have more than sufficient surface area to act as radiators, if needed. Proper choice of paint and thermal conducting surfaces will ensure that the booms radiate if they are made of heat conducting material.

The thermal control subsystem will contain the following major elements: temperature sensors, heat strips and power switcher, and TCS control logic (resides in flight computer). The flight computer is interfaced with the various temperature sensors through signal conditioners and with the power switching unit that applies power to the heat strips. The operations logic and performance characteristics were also developed during the Phase II effort.

### 5.2.7 System Characterization and Tuning Unit (SCTU)

An SCTU concept design subsystem was developed as part of the Phase II effort to provide small disturbances to the satellite subsystem elements. The SCTU subsystem purpose will provide a means of introducing known input disturbance levels and measuring either an open-loop or closed-loop response during on-orbit operations.

The SCTU was required to provide three different type disturbances either individually or in combination. The three types are PSD spectrum, waveform, and pulse. Each was required to be customizable within the following limits.

PSD Spectrum: 20 settable peaks from 0.1 to 100 Hz  
10 background noise levels 0.1 to 100 Hz  
Each bandwidth region settable  
Level and slope for each region settable

Waveform: 10 settable types 0.1 to 100 Hz  
Sine, square, sawtooth, triangle, etc., or  
Shape definable by specified points

Pulse: Pulse repetition rate and spacing settable

The disturbance level capability for each type will be determined in the follow-on design phase.

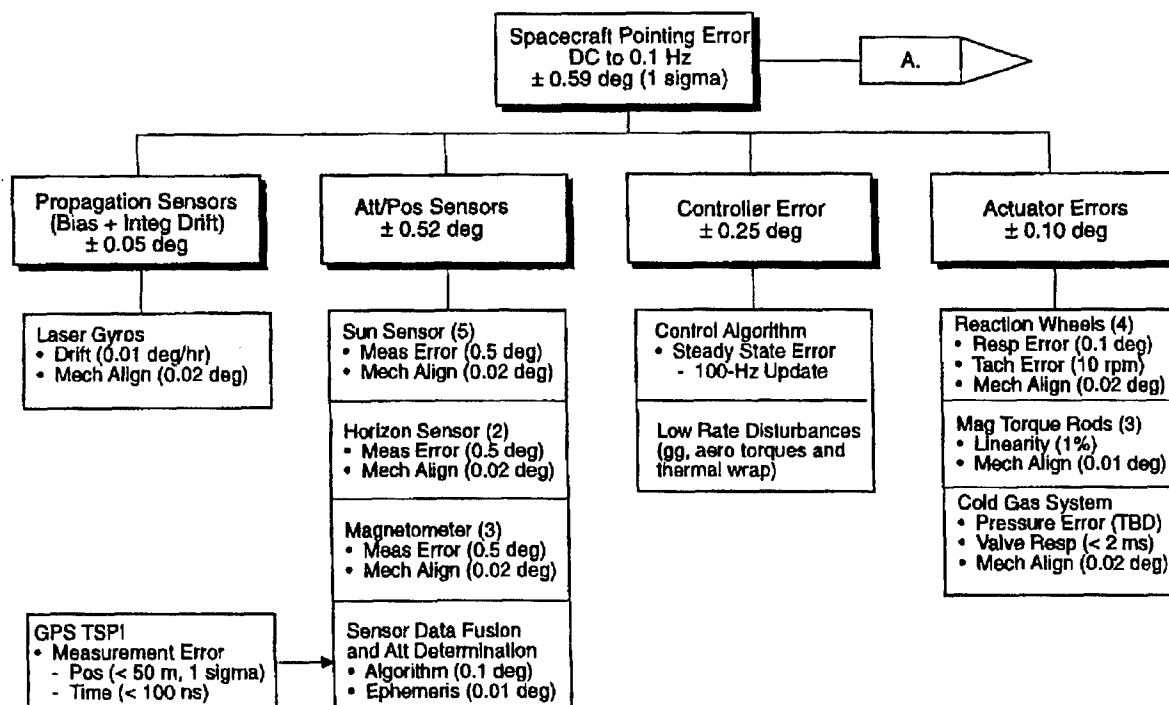
The SCTU controller was required to be a self-contained unit to store and initiate the above defined disturbance types and drive the disturbance actuators. The SCTU was designed to interface to the flight computer, and the flight computer will be able to enable the SCTU controller and reprogram the SCTU controller. The SCTU also was required to provide a feedback such that the flight computer can monitor the SCTU output to detect any error conditions and disable the SCTU.

### 6.0 PERFORMANCE MEASURES

The pointing of the LCSS is one of the most important aspect of its performance. The system performance budget is set forth in Section 3.6 of the SRD. The SRD also has set forth the pointing requirements for the spacecraft in DDB Section 4.2.3, Stabilization and Attitude Control (SAC) Subsystem, and for the payload in DDB Section 4.1.3, Payload Acquisition, Tracking, Pointing, and Stabilization. The terms accuracy, pointing error, and pointing stability are defined in DDB Section 3.2.3, Satellite Attitude.

### 6.1 SPACECRAFT PERFORMANCE

Analyses to determine the spacecraft pointing error for target acquisition are summarized in the error budget shown in Figure 6.1-1 as  $\pm 0.59$  deg (1 sigma). The associated spacecraft pointing stability is shown in Figure 6.1-2. The arrows shown as A, B, and C provide continuity by corresponding to similar arrows on Figure 6.1-3. These values lie within the bounds set forth in the SRD.



Note 1. Error Budget is WRT Optical Bench Commanded Attitude  
 Note 2. No Structural Dynamics, i.e., Rigid Body (with thermal distribution)

Figure 6.1-1. Spacecraft pointing error budget for payload target acquisition.

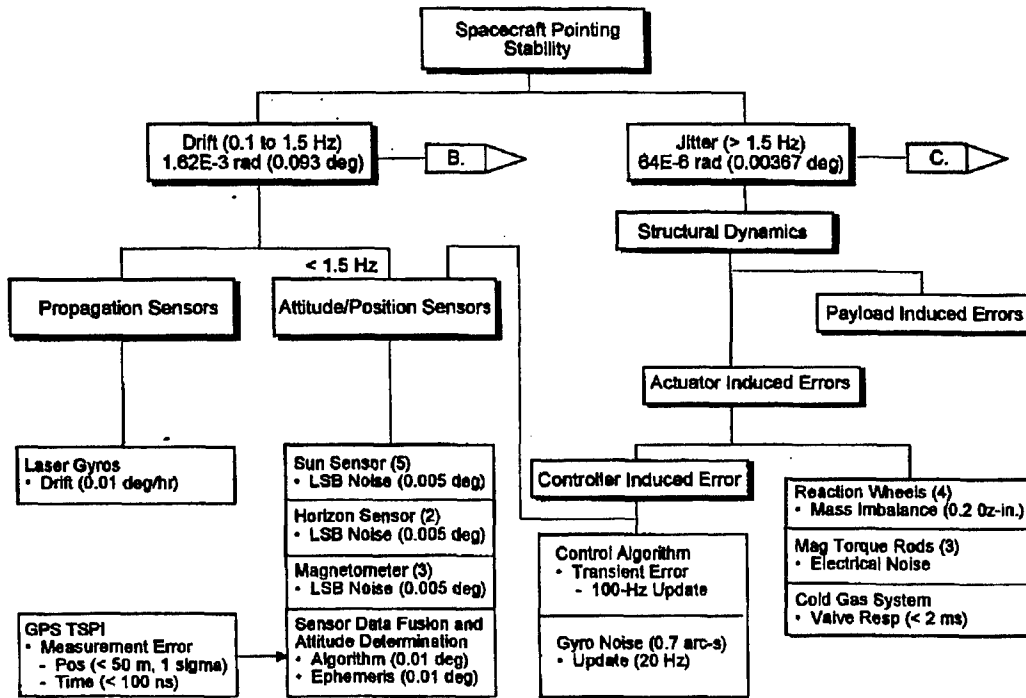


Figure 6.1-2. Spacecraft pointing stability budget for payload target acquisition.

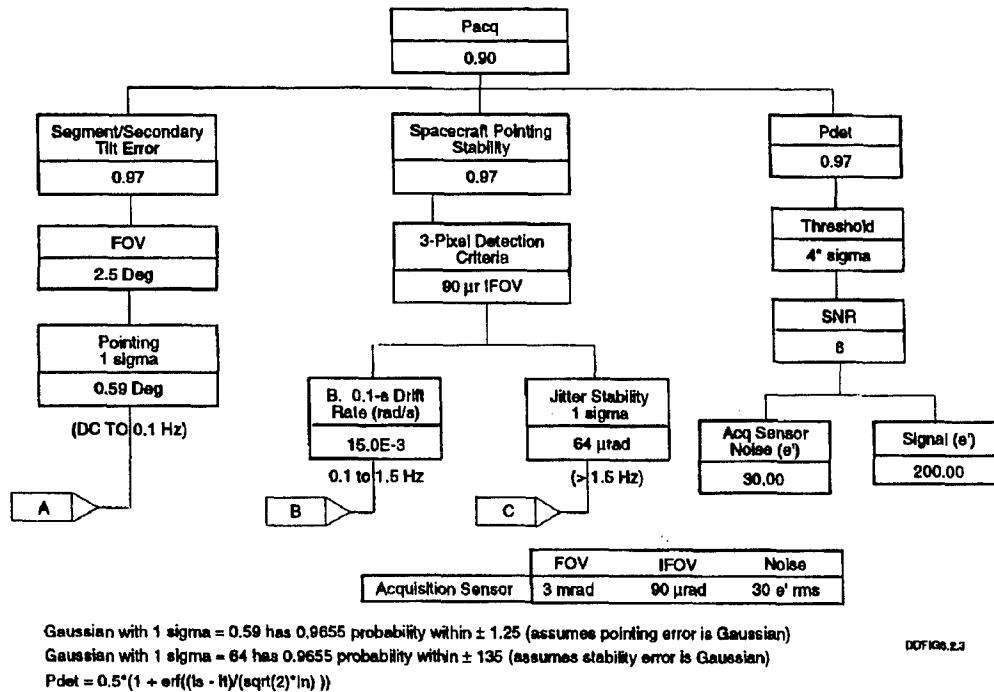


Figure 6.1-3. Acquisition camera error budget.

### 6.1.1 Flexible Control Performance

Two types of pointing performance analyses were conducted. The first investigated the flexible response of the booms during the continuous disturbance caused by the reaction wheels. The

second investigates the open-loop (no payload feedback) capability of the satellite to point the optical bench during a groundsite tracking pass.

The flexible response of the booms was investigated by constructing a Simulink simulation of the rigid optical bench in combination with a first-mode flexible model of the primary and secondary booms. The simulation is illustrated in Figure 6.1.1-1. As shown, the simulation included both stiffness and damping effects of the booms, and the response of the booms is fed back into the optical bench. The optical bench is modeled as a rigid body since its first free-free mode is at 436 Hz, and the expected first mode with payload and spacecraft system mass loading is targeted to be above 100 Hz. The simulation includes the sinusoidal (20 Hz) disturbance input of the mass imbalance of the reaction wheel (1.08e-4 ft-lb.). The first mode of each boom was modeled using a simplified flexible model. The flexible model was derived by first calculating the first cantilever mode of each boom (11.6 Hz for the secondary, and 52.8 Hz for the primary), and then solving for an equivalent spring at the base of an equivalent rigid boom that gave the same first mode slope at the tip and the correct first mode frequency. This was essentially a transfer function approach, except the model was set up to also extract the angular velocities needed to model the structural damping. This is an acceptable method for initial control system and structure interaction studies and was used by Draper Labs early in the mission planning for the STS OAST-1 mission.

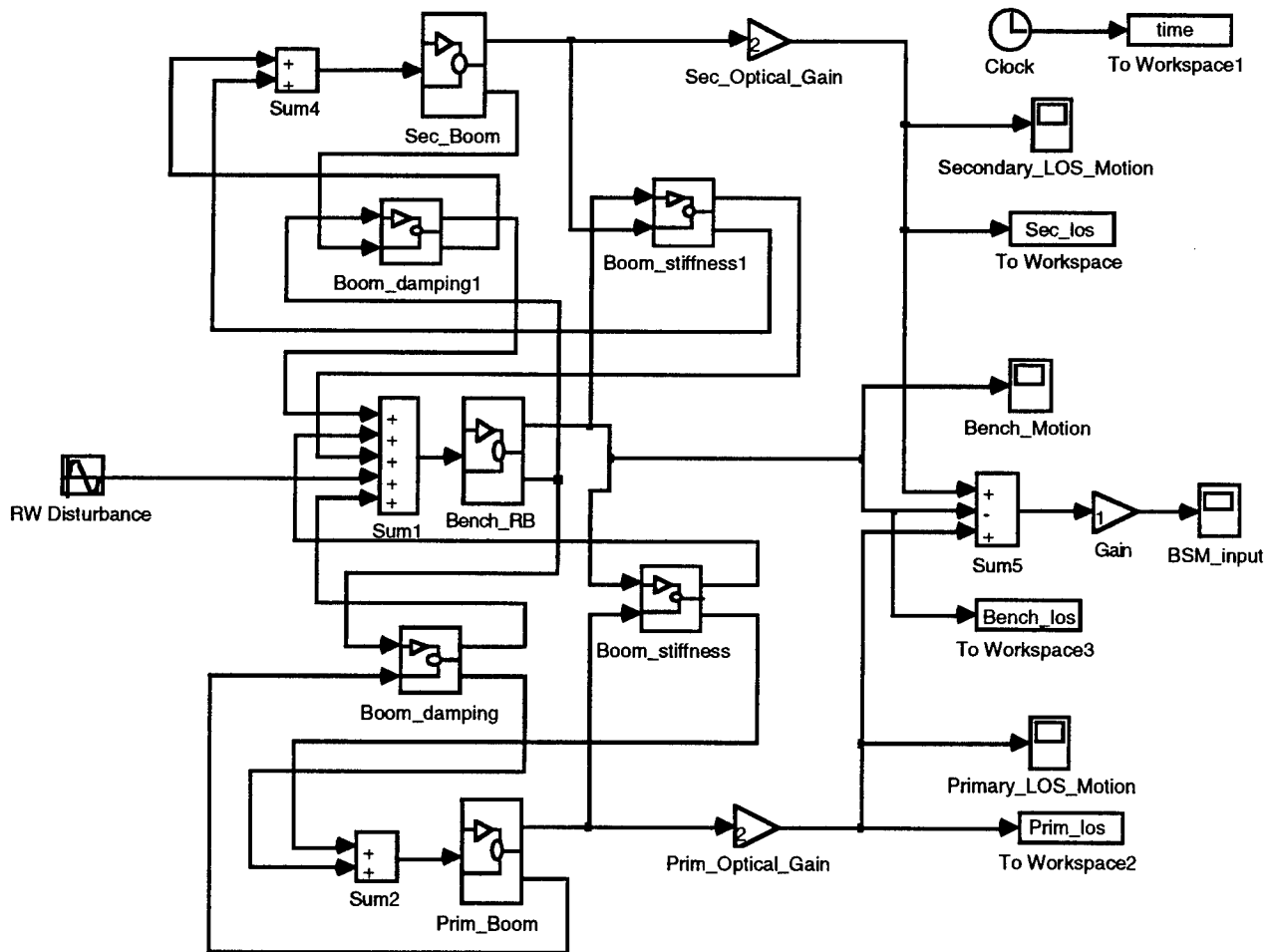


Figure 6.1.1-1. LCSS flex dynamics simulation.

The model was exercised with structural damping values of 0.5% and 1.0%. The results of this simulation can be found in Table 6.1.1-1. These values only show the maximum error from the simulation. Detailed plots of the simulation results can be found in Section 6.1.1-1 of the DDB. One phenomena found during the simulation that Table 6.1.1-1 does not reveal, was a beating motion on several of the LOS plots. This motion was later found to be caused by structural dynamic interactions between the secondary and primary mirror booms. This interaction is what caused a great deal of the LOS error in Table 6.1.1-1.

Table 6.1.1-1. LOS error from simulation.

	Boom-Mounted Primary Mirror LOS (microradians)	Secondary Mirror LOS (microradians)	Optical Bench (microradians)
0.5 % Damping	5	0.06	0.8
1.0 % Damping	1.5	0.03	0.3

The flex simulation demonstrated that the LOS motions caused by the disturbance response of the boom dynamics during a target tracking experiment will be within acceptable values (as stated in the SRD), except during a few particular large resonant periods. If boom materials are used which increase the damping to 1.0%, the large resonant periods will be mitigated.

### 6.1.2. Attitude Control Performance

The second pointing performance study investigated the capability of the reaction wheel control system to perform a groundsite tracking maneuver. The operating altitude for the study was 296 km (160 nm), which is considered the worst case end-of-mission operating altitude. The control system used was a PID controller used with rate being the proportional control. The simulation was implemented using Simulink and is illustrated in Figure 6.1.2-1. The maximum attitude error occurs when the satellite passes through the nadir point and must reverse the rate command from a maximum positive rate to a maximum negative rate. The nominal attitude error that occurs is about 0.52 mrad with a momentary spike at about 1.05 mrad.

These attitude errors are within the specified FOV of the LCSS Phase 2 payload of 3 mrad but would most probably be unacceptable for a true imaging system. For an imaging system with multiple apertures, the reaction wheel torques would be assisted with a rate boost system during the ground pass in order to keep the attitude errors within an acceptable level.

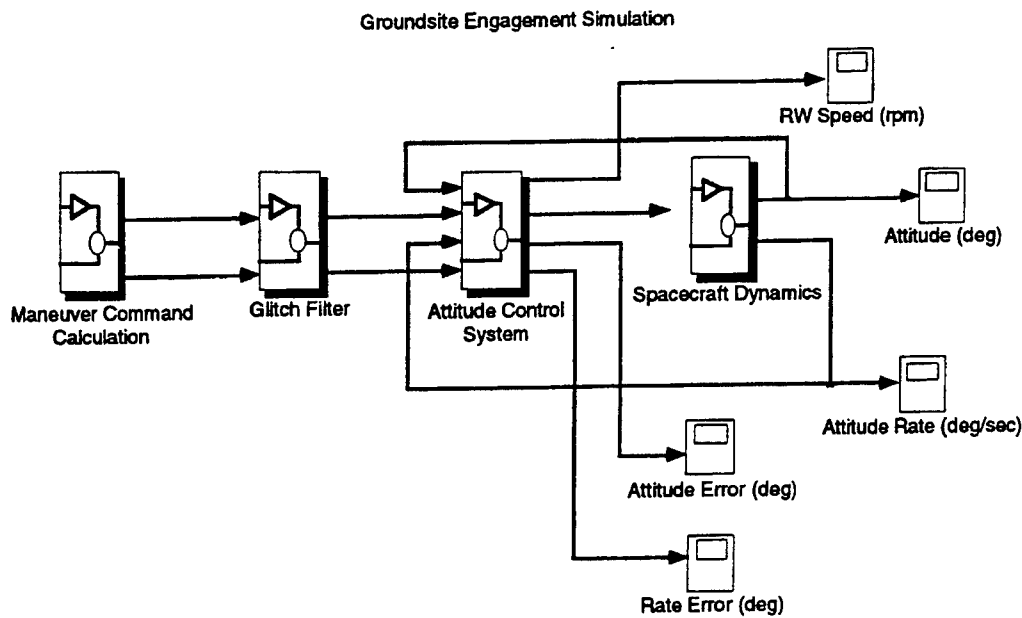


Figure 6.1.2-1. SIMULINK groundsite simulation.

## 6.2 PAYLOAD PERFORMANCE

The performance predictions include point-spread function (PSF) prediction, optical alignment error budget, acquisition error budgets, and star radiometric sensitivities

### 6.2.1 Objectives/Error Budget

In order to design the payload control system an optical alignment error budget was created. Figure 6.1-1 represents the alignment error budget. The top-level metric is fringe contrast. This is the effective fringe contrast of the object of interest as imaged onto the science camera. Since this two-aperture system produces a fringe pattern, described below, the approach in developing this error budget is to allocate error terms to alignment errors that cause a degradation in the resulting fringe contrast. The top-level fringe contrast is 0.5.

### 6.2.2 Point Spread Function (PSF)

The PSF of the two-aperture system is shown in Figure 6.2.2-1. This PSF is similar to the well known Young 2 slit interference experiment and is characterized by fringes contained within a central spot. The fringe spacing is determined by the spacing of the primary mirror segments. The diameter of the spot containing the fringes is determined by the diameter of an individual segment. The fringe spacing is found by dividing the wavelength of the incoming light by the primary mirror spacing. The fringe spacing is 238 nrad. The spot diameter is 1.3  $\mu$ rad. This results in 5.3 fringes per spot. The PSF depicted in this figure corresponds to laboratory experiment data of the image of a point source on the science camera.

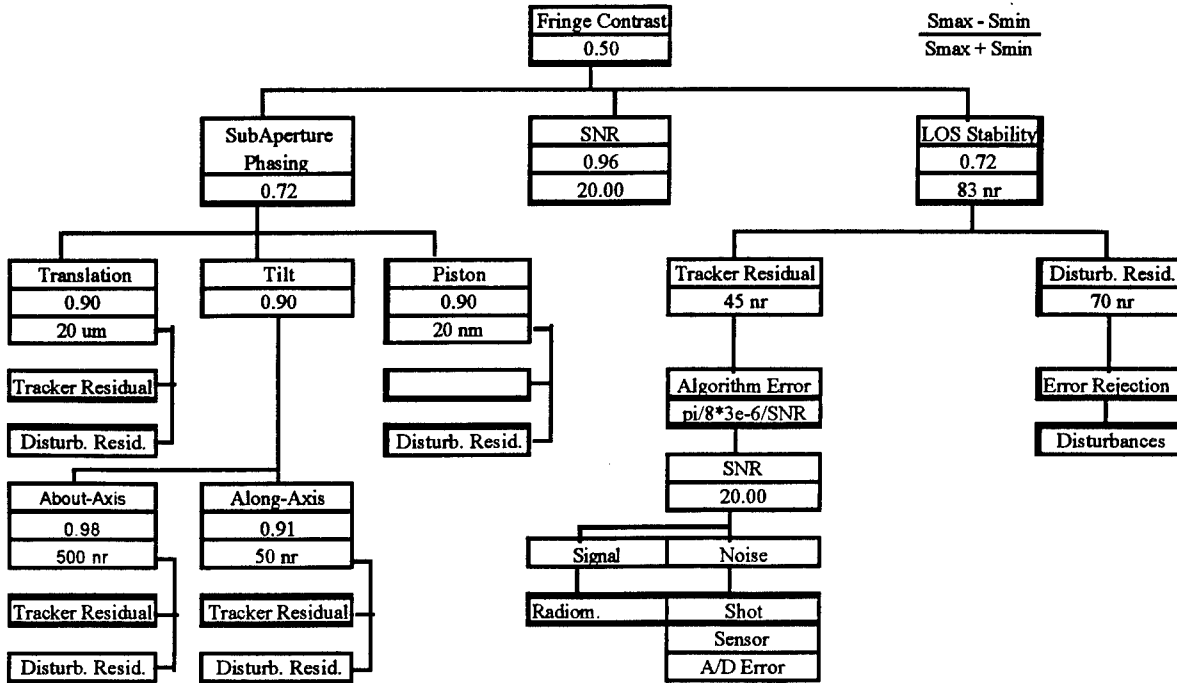


Figure 6.2.1-1. Optical alignment error budget.

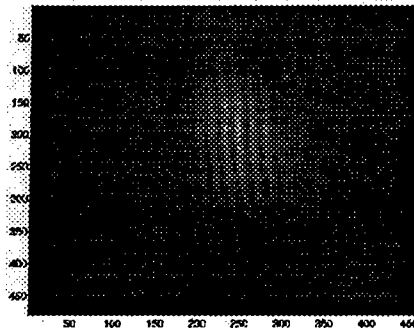


Figure 6.2.2-1. LCSS data - system PSF.

### 6.2.3 Subaperture Phasing Error Budget

A contrast of 0.72 has been allocated to the ability to phase the two subapertures. Subaperture phasing involves correcting for segment translation, tilt, and piston. The contrast allocation for these terms is all 0.9. An initial engineering estimate of 20 microns has been allocated for the translation error corresponding to a 0.1 contrast reduction. The subaperture tilt error has been divided into about-axis and along-axis contributors. The about-axis term refers to the subapertures tilting as if the primary boom was twisted about the long axis. The along-axis term refers to a tilt which causes the subapertures to point toward or away from each other. The contrast degradation is much more sensitive to errors in the along-axis tilt. A contrast of 0.91 has been allocated to the along axis term. A Matlab simulation of the two-aperture pupil function revealed that a tilt of 50 nrad will produce the 0.09 contrast degradation. A contrast of 0.98 has been allocated to the about-axis term. That same simulation has shown that 500 nrad of tilt error

will produce the 0.02 contrast degradation. The piston error term refers to the contrast degradation caused by a piston error between the two subapertures. Piston error is also known as optical path length error. Using the same Matlab simulation, a piston error of 20 nm was found to produce 0.1 reduction in contrast.

#### **6.2.4 Signal-to-Noise Ratio (SNR) and Line-of-Sight (LOS) Stability Allocation**

The degradation of contrast caused by the SNR of the image on the Science camera has been allocated to be 0.96. A contrast of 0.72 has been allocated to the LOS stability. LOS stability refers to the lateral motion of the spot on the Science camera caused by tilt jitter in the full-aperture tilt control loop. This error has been allocated between the tilt error caused by tracker noise, and unrejected disturbance residual tilt error. Translating the fringe pattern by 83 nrad will cause a degradation of on-axis contrast of 0.08. Of the 83 nrad, 45-nrad residual error has been allocated equally between the tracker error and disturbance residual. The tracker residual is found by using the quad cell track error equation using this equation, the SNR required is 20. The disturbance residual will be evaluated once the disturbance power spectral densities (PSDs) are better defined. The full-aperture tilt, open-loop cross-over bandwidth is 100 Hz.

#### **6.2.5 Acquisition Error Budgets**

Once the acquisition camera acquires the object, the spacecraft is closed-loop pointed at the object, and the telescope segments are aligned such that the intermediate tilt sensor can acquire the object. Error budgets have been developed for the acquisition camera and the payload bench intermediate tilt sensor. The purpose of both budgets are to determine alignment and SNR requirements such that acquisition of a star can occur.

##### **6.2.5.1 Acquisition Camera Acquisition Error Budget**

Figure 6.1.3-1 describes the error budget for the acquisition camera. The budget is derived with the top-level requirement of a probability of acquisition of 0.9. The budget is divided into three areas, they are; spacecraft pointing error, spacecraft pointing stability, and probability of detection. The required spacecraft pointing error is required to be small enough (0.59 deg) such that there is a 0.97 probability that the object is within the FOV of the acquisition camera. The spacecraft pointing stability is driven by the acquisition camera detection algorithm. The detection algorithm requires the object to move less than 3 pixels per frame. The probability of detection ( $P_{det}$ ) of the acquisition camera determines both a threshold setting and a required SNR of the object

##### **6.2.5.2 Optical Bench Acquisition Error Budget**

Figure 6.2.5.2-1 describes the error budget for the optical bench. The optical bench budget is set up very similar to the acquisition error budget. Instead of spacecraft pointing, the optical bench acquisition relies on the telescope primary segments and secondary to be tilted accurately and stable. The  $P_{det}$  criteria is again used to determine threshold settings and SNR requirements.



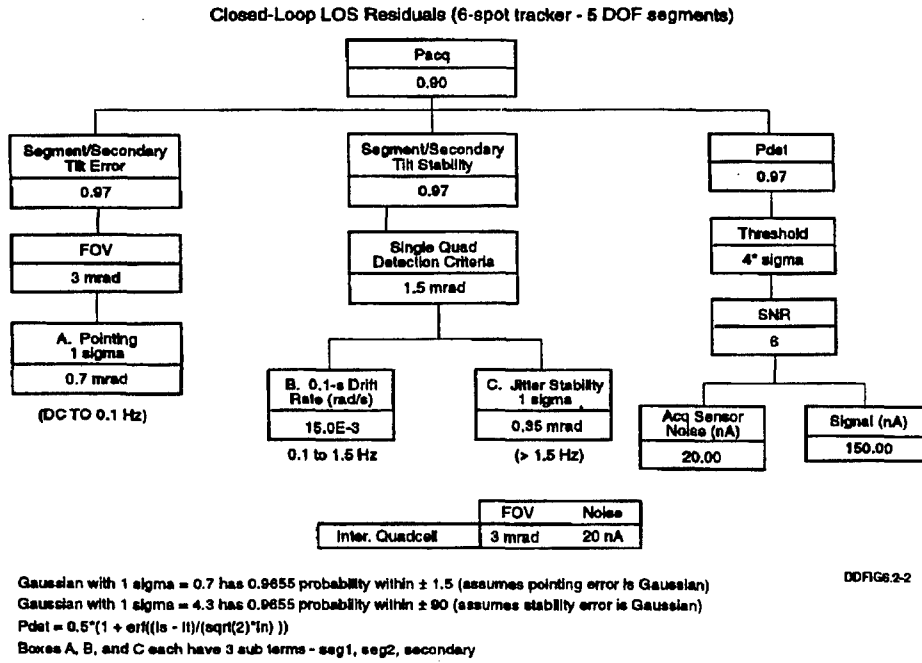


Figure 6.2.5.2-1. Optical bench acquisition error budget.

### 6.2.6 Radiometric Sensitivities

The radiometric sensitivity of the LCSS two-aperture system to stars is shown in Figure 6.2.6-1. The radiometric calculations were done for the acquisition, intermediate tilt, and science cameras only, as these are the only sensors which sense the star as a source. The assumptions used for the SNR calculations can be found in Section 6.2.4 of the DDB. Figure 6.2.6-1 shows that the star magnitude needs to be at least 5.5 for all sensors to have an SNR of at least 10

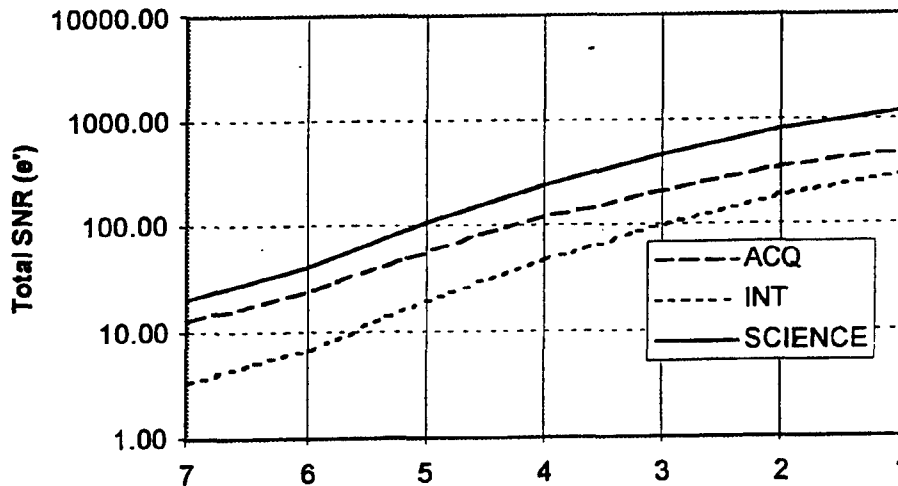


Figure 6.2.6-1. Radiometric sensitivities of the LCSS two-aperture system.

### 6.3 SATELLITE MASS PROPERTIES

The current estimated satellite mass broken down by subsystem is shown in Table 6.3-1. A more complete breakdown of the subsystems weights can be found in Section 6.3 of the DDB. The goal of keeping the weight at about 204 kg should be attainable with proper design. Refinement of these values is TBD.

Table 6.3-1. Subsystem breakdown of the satellite mass.

Subsystem	Weight (kg)	Weight (lb)
Attitude Control System	36.11	79.63
Disturbance Generator	2.48	5.5
Electrical Power System	36.56	80.6
Flight Computer	4.97	11
Thermal Control	1.59	3.5
Telemetry	13.71	30.23
Structure	61.23	135
Payload	47.64	105
<b>Total</b>	<b>204.3</b>	<b>450.46</b>

### 6.4 ORBITAL PERFORMANCE

Orbital decay analysis of the LCSS concept was also performed. The mission lifetime goal was set to be a minimum of six months. Using an energy method calculation along with several other assumptions listed in DDB Section 6.4, decay rates were calculated as shown in Table 6.4-2

Table 6.4-1. Decay times vs. altitude.

Altitudes	Decay Times (days)
376 km to 370 km	23
370 km to 333 km	125
333 km to 296 km	34
296 km to 259 km	25
259 km to 222 km	17
222 km to 185 km	14

### 6.5 MASS EXPULSION SYSTEM MARGINS

This will be determined in the next design phase. The margins are dependent on detailed experiment requirements which will be defined in the next design phase.

### 7.0 LABORATORY EXPERIMENT

As part of the risk-reduction piece of the Phase II LCSS project, a laboratory breadboard experiment was completed to test the feasibility of the payload system. The main goal of this effort was to see if phasing of the two sparse-aperture primary mirrors could be accomplished.

#### 7.1 EXPERIMENT BREADBOARD DESCRIPTION

The breadboard experiment system includes an optical design, steering and piston mirrors, and a computer system to close loops and acquire data.

##### 7.1.1 Breadboard Optical Design

The layout of the payload breadboard experiment is shown in Figure 7.1.1-1. The scale of the breadboard sparse-aperture telescope is 1/4 of the satellite payload telescope diameter. Although the sparse-aperture telescope size is not the same size as the payload design (2.1-m effective diameter), all elements following the first beam reduction telescope (BRT1) are the same scale as the satellite payload design. This is achieved by changing the magnification of BRT1 from 8.7 x (satellite) to 2.2 x (breadboard). The dotted line in Figure 7.1.1-1 represents the reference beamline. The layout accomplishes the independent steering and pistoning of one beamline with respect to the other with the fixed mirror M2 and tilt/piston mirror BSM2 pair.

The telescope design is a Schwarzschild type. Originally, an afocal design was chosen. However, the afocal design required a source collimator with a diameter greater than 625 mm, which was not available. Therefore, the finite conjugate design shown in Figure 7.1.1-1 was selected.

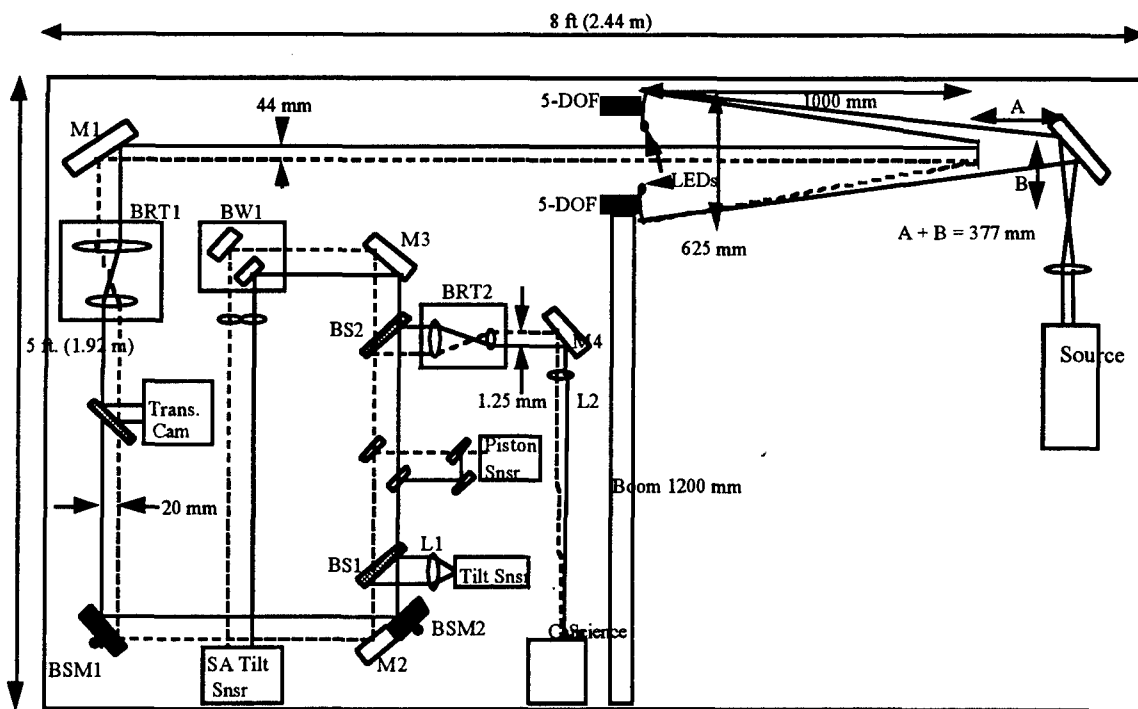


Figure 7.1.1-1. Breadboard experiment optical layout.

### 7.1.2 Sensor Descriptions

Table 7.1.2-1 lists the parameters of the sensors on the Breadboard experiment bench.

Table 7.1.2-1. Sensor parameters.

Sensor	Sensor Type	Model	Lens Fl *	FOV *	BW
Tilt Sensor	Si LEC	UDT SC/10 D	25 mm	23 deg	2 kHz
Sub Aperture	2 Si LEC	UDT SC/10 D	1.0 m	10 mrad	2 kHz
Piston	Si LEC	UDT SC/10 D	na	na	2 kHz
Science Camera	Si FPA	Fairchild CAM3000	12.8 m	1 mrad	60 Hz

\* Lens Fl and FOV in steering mirror space (Science Camera has 16x BRT in path)

The piston sensor is made up of 3 50/50 beamsplitters, 1 mirror and a Si Lateral Effect Cell (LEC). The Si LEC, which is used purely as an intensity measurement device, and electronics have a 1000-Hz bandwidth. Two of the beamsplitters sample the beamlines, and the final beamsplitter is used to superimpose the beamlines for the Si detector. The beamlines are tilted and translated such that the intensity pattern on the sensor is uniformly bright or dark in response to piston of 1/2 wave. The piston sensor images the system pupil and therefore has no real field-of-view.

### 7.1.3 Steering Mirrors

The LCSS uses two steering mirrors to control the two tilt loops. BSM #1 is a Burleigh PZ-90, 2-inch steering mirror and BSM #2 is a Burleigh PZ-80, 1-inch steering mirror. The steering mirrors use three segments of a piezoelectric tube to provide tilt-free translation and angular motion. The piezoelectric actuators have a flat response out to 5 KHz, but when the mirrors are attached to the drivers, the response of the system changes. We noticed that the response of the mirrors and the actuators had some modes which could affect how high a closed-loop bandwidth one could achieve. The actuators had a total stroke of 6 micrometer with a sensitivity of 6 micrometer/1000V axially with a linearity better than 5%. The three piezoelectric actuators are seated in a cylindrical aluminum housing. By driving the three actuators appropriately, one can achieve X and Y tilts as seen at the LEC, and by driving the actuators simultaneously one can piston the beam.

The mirror actuators are driven by voltages from 0 to 1000 Vdc which is converted from a 0 to 10 Vdc voltage source via a high-voltage amplifier.

### 7.1.4 Computer Systems

An integral part of the LCSS laboratory experiment is a multi-tasking embedded controls, data acquisition and mode logic decision making computer system. This computer system contains eight channels of analog-to-digital conversion, eight channels of digital-to-analog conversion and the capability to acquire data on both analog and digital system signals simultaneously. Experiment mode control is performed autonomously while the experimenter monitors hardware and software state. The experimenter can override the autonomous sequencing and set the experiment mode manually. The computer closes three digital tip/tilt mirror control loops and drives piston motion on the third mirror while closing all 100-Hz tip/tilt control loops. The computer system hardware and decision making software have been designed and implemented to automatically measure and calculate optical and electrical subsystem scale factors. This automatic calculation of critical system parameters allows the experiment control system to be much less sensitive to optical alignment, optical component layout and accuracy of experimenter measured system constants and scale factors.

The LCSS experiment computer system consists of six VME form factor computer cards contained in a VME chassis and interconnected to the photo detectors, control mirrors and visible band focal plane sensor. The system's single CPU is a Motorola MVME167 single-board computer containing a MC68040 CISC. Eight channels of analog output are provided by a single VMIC 4116 16-bit digital-to-analog converter card. The VMIC 4116 is connected directly to the six steering mirror axes by RG-58 coaxial cables. The DAC has a specified conversion latency of 10 micro-seconds. All channels of the digital-to-analog converter are updated simultaneously so that the conversion delay is only incurred once for all eight channels. Analog-to-digital conversion is provided by two custom fabricated VME system cards. Eight channels of analog signal sensing and conversion are provided by the first of these boards, the acquisition card (ACQ). The ACQ card performs analog voltage sensing, signal offset adjustment and signal dynamic range adjustment through the use of programmable gain stages. Four pole switched capacitor filters are available for each signal independently and can be used for anti-aliasing or signal noise filtering applications. The second component in the analog acquisition system is a remote signal conditioner (RSC) circuit card. The RSC contains a MC68332 embedded controller that is responsible for configuring the ACQ card and its independent channels and acquiring the digital data from the ACQ card and presenting it to the buss controlling CPU at specified VME addresses. The availability of the 68332 processor offloads the main CPU from having to clock and configure the analog system and allow much higher bandwidth control processing by lowering the analog data latency as seen by the controls processor. The data acquisition system also has the somewhat unique capability to perform auto-calibration. Each analog channel can selectively be connected to an on-card precision calibration DAC. Once connected to the known analog signal the channel voltage is measured and the offset and gain amplifiers are programmed to remove channel biases prior to full system operation. The resulting offset and gain values are presented to the CPU at VME locations and are subsequently used to convert the analog signals to engineering units. By performing an auto-calibration both before and after experiment operation, information can be obtained to determine sources of system errors and precisely measure changes due to thermal/electrical variations in the sensors. The analog-to-digital system is connected directly to the experiments three position sensing photo detectors. The remaining two components of the computer system are used to acquire and process video image data from

the experiments visible focal plane. RS-170 video is digitized and processed to determine the intensity and relative locations of the two laser beams incident on the focal plane. A Datacube MaxVideo 200 pipelined image processing board is used to acquire and process the video signal and update the control system at full frame rate.

The computer software used to acquire data, control mirror tip/tilt and piston and perform the image processing of the RS-170 video signal consists of approximately 10,000 lines of C source code. A tree breakdown of the C code is shown in Figure 7.1.4-1. The computer system utilizes the VxWorks real-time operating system and the Datacube Imageflow libraries for configuring the MaxVideo 200 and performing the full rate video image processing. The computer software architecture consists of several hierarchical levels of system source software. Low-level device drivers have been created that allow hardware to be configured and initialized. Intermediate-level software performs digital control loop compensation and fast image processing calculations. Auto-calibration and system configuration software performs system level integration and test functions and calculates all system parameters and scale factors in real-time each time the experiment is operated.

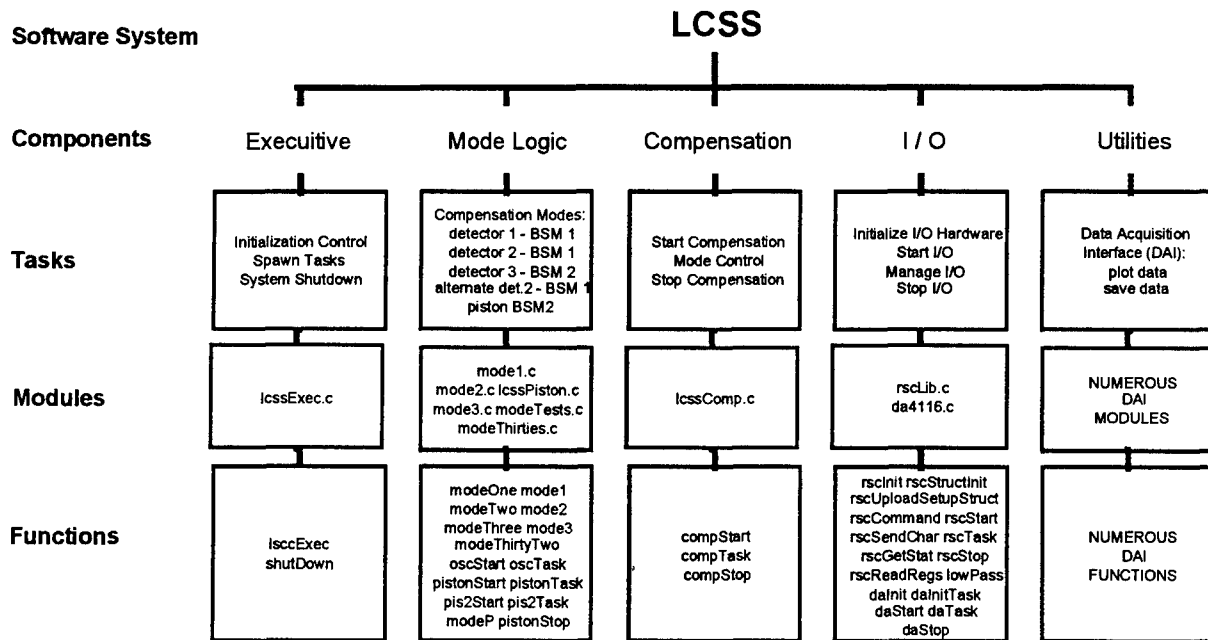


Figure 7.1.4-1. Tree breakdown of software.

High-level software mode logic and decision making software has been written that allows experiment operation and decision making in an autonomous mode, reducing operator errors and reliably exercising the experimental system. The auto-calibration software has proved well worth its development time through savings in experiment configuration time and relative insensitivity to small system changes. A VxWorks add-on software package called StethoScope is used to perform the real-time data collection and storage of both digitized analog signals and software

variable critical to determining system performance and troubleshooting. The software used to process the video imagery has been developed over the past year for use in highly dynamic target tracking and inspection system image processing. Consisting of well over half of the custom software in the system, the image processing software provided a large advantage to the overall development of the LCSS experiment software.

**7.1.5 Boom**

In order to have the future capability to validate the control architecture under dynamic disturbances, a boom was included in the laboratory experiment. Like the spacecraft payload design, the boom was to have one of the telescope primary mirror segments attached to it. The other end of the boom was rigidly mounted to the optical bench. The boom characteristics are shown in Table 7.1.5-1 and was built with material on hand at AF PL/VTSC.

Table 7.1.5-1. General boom characteristics.

Parameter	Value
Length	47.25 in.
Diameter	7 in.
Wall Thickness	0.060 in.
Weight	11b 14 oz.
Material	Byle Technologies IM-7/BTCy-1A Tow Preg for 90 deg piles IM-7, 150 GSM/BTCy-1a Unitape for the 0 deg piles (toughened epoxy resin)
Layup	6 piles [90/0/0/0/0/90]
Tooling	7 in x 6 1/2 in chrome plated stainless steel tubing for the mandrel
Bagging	a) 1-in. wide nylon webbing b) shrink tape c) bleeder cloth d) polyimide bagging film
Modulus	17.2 Msi
Deflection	34 microns

Figure 7.1.5-1 shows a schematic of the boom setup used in the lab. The boom apparatus consists of a stand, two interface pieces, two tubular members and the boom. All of the boom apparatus parts are made from 2024-T6 aluminum except the boom, which was made from graphite fibers.

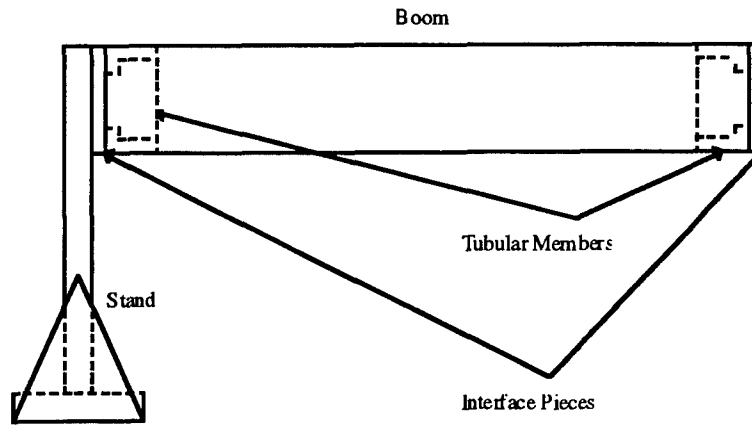


Figure 7.1.5-1. Picture of the boom apparatus (not to scale).

## 7.2 CONTROL LOOPS

The optical system is phased by controlling tilt, translation and piston of the optical system. By using two primary segments, the optical path of one segment is used as a reference, and the other optical path is controlled to the reference. The optical and control architecture is shown in Figure 5.1.1-1.

### 7.2.1 Operation Sequence

Translation control of the primary segments is performed by moving the primary segments with motorized stages. One LED is attached to each primary segment at the edge. The LEDs are imaged onto the translation camera. The primary segments are translated such that the images of the LEDs are aligned to empirically determined optimum locations on the translation camera. Once the translation control has been optimized, the translation stages freeze holding their last commanded position. By utilizing the shallow depth of field properties of the translation camera, translation control of the primary segments along the optical axis (z axis) of the system is controlled by finding the optimum focus location of the images of the LEDs on the translation camera. Once the optimum focus for each primary segment is found, the z-axis control of each segment is also set to freeze holding their last commanded position.

At this point, the LEDs are turned off, the on-board laser is turned on, and the translation camera lens system is set for infinity focus. With the lens system in this position, the laser return from the primary segments imaged onto the translation camera represents the tilt of the primary segments. Using empirically determined optimum locations for the laser intensity onto the translation camera, coarse tilt control of the primary segments can be achieved. This two-axis-per-segment tilt control can either be set to freeze holding last commanded position or can run in closed-loop control, depending on the disturbance environment of the particular engagement.

To close the subaperture tilt control loop, first acquire the spot with subaperture tilt sensor number 1. Using BSM1, close the track loop to center the spot. Next, acquire the second spot using subaperture tilt sensor number 2. Close a track loop around subaperture tilt sensor 2 and



BSM2. A novel control technique, described below, was designed to prevent the loops from "fighting". These two tilt loops both have 100-Hz open-loop crossovers.

The next step is to acquire with the piston sensor and perform piston alignment between the science camera and piston sensor. Verify appropriate signal intensity on piston sensor. Both beams are now overlapped on this sensor. To acquire the piston error signal, scan the coarse piston mirror drive to find peak intensity output of the piston detector. Hold (i.e. freeze) the coarse piston mirror at this position. The OPD between beam 1 and 2 is now within 1/2 wave. Once 1/2-wave error is achieved, fine-track piston control can be entered. Fine piston control is done using the piston dither, 8-bin algorithm described below. Remove laser line blocking filter from the science camera. Scan the initial alignment control and simultaneously compute fringe contrast of science camera. While the initial alignment control is scanning, the fine-track piston control off-loads to coarse drive. Once peak fringe contrast is found on the science camera, the initial alignment controls is set for hold/cage position. The piston sensor and science camera are now piston aligned. The laser line blocking filter is now reinserted in front of the science camera.

### 7.2.2 Tilt Control

The tilt control for the LCSS system is conceptually simple. A simplified diagram is shown in Figure 6.3.2-1.

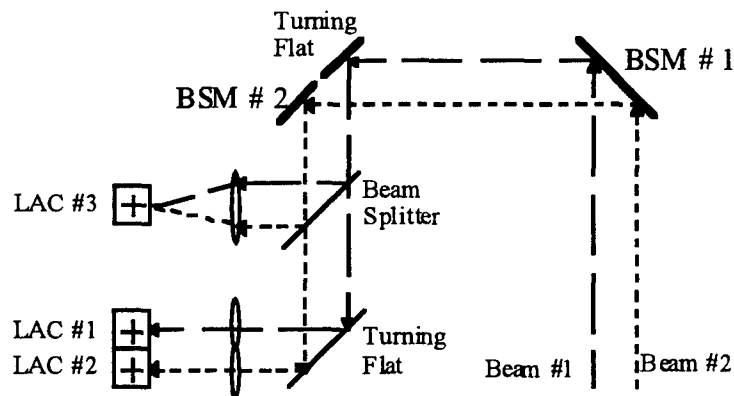


Figure 7.2.2-1. LCSS tilt loop setup.

The two beams of light, indicated in Figure 7.2.2-1 as Beam #1 and Beam #2 hit Beam Steering Mirror (BSM) #1. They are reflected to the two mirrors at the top left of Figure 7.2.2-1. Because of the physical separation of the two beams, Beam #1 reflects off a turning flat while Beam #2 hits BSM #2. The beams then hit a beamsplitter, where some of their energy is focused onto LEC #3. The rest of the light continues through the beamsplitter to a turning flat. The two beams are then focused onto two LECs, listed as LEC #1 for Beam #1 and LEC #2 for Beam #2.

Each of the LECs represents a control loop. LEC #3 is used for low-bandwidth alignment. This is a 10-Hz loop which uses BSM #1 to center the focus of the two beams onto LEC #3. The assumption is that if the spot is centered on LEC #3, then the two beams will fall within the FOV of LEC #1 and LEC #2. At that point, control of BSM #1 is turned over to a high-

bandwidth loop. LEC #1 and LEC #2 use BSM #1 and BSM #2 to close high-bandwidth loops (100 Hz) to eliminate the optical tilt of Beams #1 and #2. Correct high-bandwidth control of the tilt loops is essential in order to correctly do the piston control.

The control functions are complicated by the devices used. The LECs yield information in two axes, referred to as x and y, while the BSMs are controlled by three piezoelectric actuators which are 120 degrees apart behind the mirror.

Calibration of each of the BSM's three piezoelectric actuators involved applying 10 volts to each of the actuators separately in tests of the mirrors response. The x and y beam movement on the LEC due to each actuator's movement was then measured and a matrix describing the BSM actuator commands to tilt output was found. Each BSM's matrix was used in the control loops to command pure x- or y-tilt to the actuators by passing the tilt commands through this transformation matrix to get BSM actuator commands. Cross coupling of the calibration was tested and only 5% leakage was found between the tilt commands.

One complication in the control loops is that while BSM #2 controls Beam #2, and BSM #1 controls Beam #1, Beam #2 also is reflected off of BSM #1, so the effect of controlling Beam #1 has an undesired effect on Beam #2. This is overcome by using a slaving technique to offset the commands given to BSM #1. The idea is to give BSM #2 a compensating command which offsets the effect of the BSM #1 command. For example, if BSM #1 was going to tilt the beam in the x direction 20 mradians to the left, then BSM #2 would issue a command to tilt the beam in the x direction 20 mradians to the right. The net effect seen at LEC #2 would be that the beam doesn't move. In order to implement the slave scheme, one needs to know the relationship between BSM #1 and LEC #2. Since we already know the relationship between BSM #2 and PP #2, any command that BSM #1 issues can be run through a transformation matrix to BSM #2 which compensates perfectly, again within the limits of the device linearities and hysteresis. Negation of this effect was found to be within 5%.

The actual controllers were merely integrators with the appropriate gains to yield the desired bandwidths.

### 7.2.3 Fine Piston Control

The sensing method was changed to sensing the intensity output of the piston detector. The intensity output is maximum when both beams are in phase and is minimum when both beams are 180-deg. out of phase. An intensity value in between the minimum and maximum is selected as the closed-loop set point. By not picking the minimum or maximum as the set point, complicated peaking algorithms are not needed. Since the science camera wants to see both beams in phase, a path length adjustment is needed to one of the beam paths. This allows the piston detector to close a loop in the linear intensity region and the science camera to observe both beams in phase.

Figure 7.2.3-1 is a block diagram of the closed-loop control for piston. The output of the piston sensor is summed in with a set point. The output error is integrated. The K/s term represents an

integrator with gain. This command is then sent to all three actuators of the subaperture tilt/piston mirror.

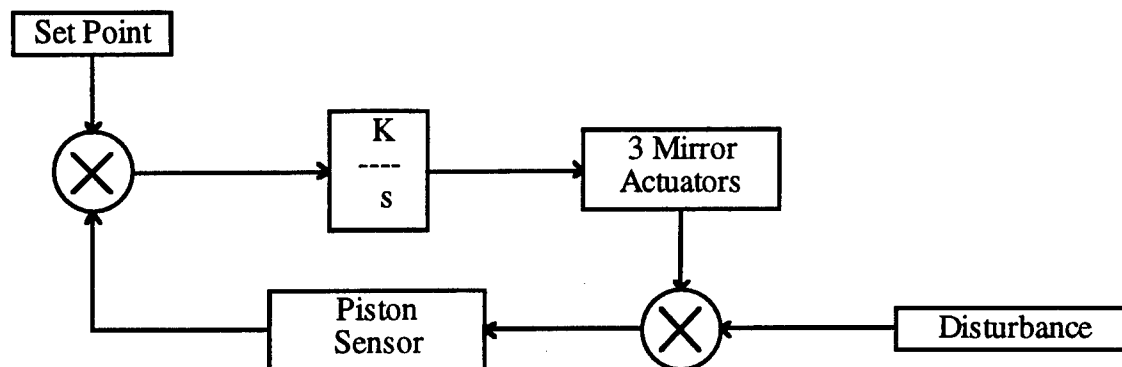


Figure 7.2.3-1. Piston sensing algorithm.

### 7.3. TEST RESULTS

Testing of the system performance involved taking measurements with and without certain parts of the telescope. The two basic test setups were the pseudo-aperture test setup (no telescope and no boom) and the telescope setup with the boom. In addition to the closed-loop BSM measurements, radial and transverse translation sensing of the primary mirrors using the Opti-Trak 100 with the LEDs was performed.

Noise measurements of the sensors were taken before and after each test run. Performance measurements of the system were taken with the full-aperture tilt loop closed, both the full and subaperture tilt loops closed, the piston loop closed and all of the control loops closed. Conversion of the LEC sensor data into microradian (tilt) was accomplished using conversion factors found by calibrating the sensors in open-loop. Data from the piston sensor was difficult to extract due to the very low SNR found during sinusoidal actuation of BSM #2 calibration testing. Closed-loop measurements for the piston testing were taken from the mirror actuation data.

#### 7.3.1 Disturbance Environment

Initial disturbance data taken from each of the cells showed a significant disturbance level from the sensors. Table 7.3.1-1 shows values found for the disturbance data from the two setup measurements.

Table 7.3.1-1. Disturbance environment.

Sensor	rms Noise Level	
	Pseudo-Aperture Test Setup (microradians)	Telescope Test Setup (microradians)
Full Aperture, X Dir.	15.0	39.8
Full Aperture, Y Dir.	7.0	39.6
Subaperture, X Dir.	13.4	43.7
Subaperture, Y Dir.	12.5	17.2

During closed-loop measurements of the system, it was found that the disturbance frequencies were at high enough levels to suggest that the sensors were very noisy and/or the environment was very noisy.

### 7.3.2 Pseudo-Aperture Test Results

The test setup for the pseudo-aperture system is shown in Figure 7.1.1-1 minus the boom and telescope. A 4-inch diameter collimator and an aperture plate with two appropriately sized holes were used for the pseudo aperture. Testing for this setup concentrated on examining the performance of the systems internal to the LCSS flight experiment. Measurements included full and subaperture closed-loop testing and closed-loop piston error measurement.

Results from the tests are shown in Table 7.3.2-1. PSDs and backsums of the data were also performed on the data to determine the dominant error frequencies. Comparing the closed-loop data with the open-loop data, it was found that there were similar power spikes at several frequencies, but no conclusions could be made due to the inconsistency of the power levels from sample to sample.

Master/slave techniques were originally tried on BSM #1 and BSM #2 due to problems of BSM #1's ability to affect both LEC outputs, but this was found to be unnecessary.

### 7.3.3 Full System Test Results

The test setup for the full system is shown in Figure 7.1.1-1. Testing for this setup concentrated on examining the performance of the optical system with significant structural components in the optical train. Measurements included full and subaperture closed-loop testing and closed-loop piston error measurement.

Table 7.3.2-1. Pseudo-aperture test results of the lab experiment.

	Pseudo Aperture Test Set-Up	
	X Dir	Y Dir
Full Aperture Tilt Control, Full Aperture (microradians)	15.7	6.8
Sub Aperture Tilt Control, Full Aperture (microradians)	11.9	6.9
Sub Aperture Tilt Control Subaperture (microradians)	15.4	14.2
Piston Control (nanometers)	7.6	
Simultaneous Tilt & Piston Control, Full Aperture (microradians)	15.1	7.1
Simultaneous Tilt & Piston Control, Subaperture (microradians)	17.4	13.4
Simultaneous Tilt & Piston Control, Piston (nanometers)	43.7	

Results from the tests are shown in Table 7.3.3-1. Again, PSDs and backsums of the data were performed on the data to determine the dominant error frequencies. Comparing the closed-loop data with the open-loop data, it was found that there were similar power spikes at several frequencies, but no conclusions could be made due to the inconsistency of the power levels from sample to sample.

Table 7.3.3-1. Full system test results of the lab experiment.

	Full System Test Set-Up	
	X Dir	Y Dir
Full Aperture Tilt Control, Full Aperture (microradians)	34.0	42.6
Subaperture Tilt Control, Full Aperture (microradians)	34.0	40.9
Subaperture Tilt Control Subaperture (microradians)	14.5	9.1
Piston Control (nanometers)	50.5	

### 7.3.4 Translation Sensing

This test involved two parts: one, error budget verification of the translation of the mirrors in fringes per meter of translation and two, measurement of the LED resolution capability of the Opti-Trak 100. Combined results from these two measurements determined whether the Opti-

Trak 100/LED system could successfully sense movements of the primary mirrors on the order of the error budgets.

#### 7.3.4.1 Error Budget Validation

Table 7.3.4.1-1 shows representative values for the radial movement of primary mirror #1 for the error budget validation test. Transverse movements and radial movement of primary mirror #2 were assumed to be around the same values.

Table 7.3.4.1-1. Error budget verification of the fringes per meter resolution with a result of 0.55 wave per micron.

Mirror Movement (microns)	Number of Fringes	Resolution Capability from Null to Peak (microns)	Wave per Micron
5	5	0.5	1
5	2	1.25	0.4
10	5	1.00	0.5
10	2	2.5	0.2

Since the approximate allocation for fringe contrast degradation due to translation is 0.1 wave of error, the corresponding translation allocation is  $0.1 / 0.55$  wave/micron, or 180 nm. However, this value should be treated as an extremely conservative upper limit since the test procedure induced a tilt as well as a translation. For the procedure to have introduced a pure translation the test would have had to have been performed with the tilt controls closed.

#### 7.3.4.2 Translation Measurement Accuracy

Determination of translation accuracy involved taking a series of measurements to extract the necessary information. First, the resolution capability of the Opti-Trak 100/translation camera system in millimeters per pixel was determined by measuring a change in the number of pixels over a set primary mirror translation. Second, using the resolution information, the rms error in millimeters was determined by measuring the rms error in pixels.

Results from the resolution test are shown in Table 7.3.4.2-1. Both radial and transverse testing of Primary Mirror #2 showed values above the predicted 22.5 microns per pixel resolution capability. Testing of Primary Mirror #1 was assumed to be on the same order of magnitude as Primary Mirror #2. Initial calibration of the system revealed an SNR of 35.

Table 7.3.4.2-1. Resolution capability results for primary mirror #1.

	<b>Mirror Movement (mm)</b>	<b>Change in the Number of Pixels</b>	<b>Scale Factor (mm/pixel)</b>
<b>Radial</b>	11.75	4.5	2.6
<b>Transverse</b>	12.7	6.55	1.9

Results from the Opti-Trak 100 test are shown in Table 7.3.4.2-2. Data sets of about 30 seconds and 514 data points were taken using the Opti-Trak 100 to demonstrate the systems ability to track the primary mirror movement. Although testing discussed in Section 5.4.2.1 of this report indicates that a smaller value of measurement error may be required, the best results achieved (19 microns rms) do meet the initial error budget translation error allocation of 20 microns (see Figure 6.2.1-1).

Table 7.3.4.2-2. The rms values of Opti-Trak 100 tracking error.

	<b>rms Error (pixels)</b>	<b>rms Error (mm)</b>
<b>Primary One, X Direction</b>	0.0073	0.0189
<b>Primary One, Y Direction</b>	0.0174	0.0330
<b>Primary Two, X Direction</b>	0.0568	0.1478
<b>Primary Two, Y Direction</b>	0.0328	0.0624

## 8 CONCLUSIONS

The three main objectives of the LCSS Phase II effort, (1) expansion of the design from the conceptual to the concept design level, (2) the demonstration of the payload system in a laboratory breadboard experiment, and (3) commercialization of the LCSS concept, have all been met. In many cases, the original Phase II objectives have been exceeded

The expansion of the LCSS design from a conceptual design to a concept design has culminated in the generation of the DDB and SRD. Both of these documents will serve as an all-in-one description of the concept design and system requirements. These documents are also complete in their description of the LCSS system and can easily be expanded in the future to add more detail as it becomes available. Also as part of this effort, several risk-reduction concept designs were completed and included in the DDB.

In addition to the concept design effort, a laboratory breadboard experiment of the optical payload was completed. This experiment successfully demonstrated the feasibility of the LCSS concept. Experimental testing of the system revealed that phasing and tilt error of a sparse-aperture telescope system could be resolved to a high degree of accuracy. The rms errors in the

system were within an order of magnitude of the error budget specifications. The pseudo-aperture test setup successfully showed that the errors budgets could be met. For the full system that included the boom and the telescope, translation sensing using the Opti-Trak 100 was within the error budget specifications and tilt and translation control was within an order of magnitude of the error budget. Improvements in the sensor quality and minor adjustments to the system design such as the inclusion of a beam reduction telescope could solve many of the difficulties with the tilt and piston control.

The experiment also showed the effectiveness of the Opti-Trak 100 commercial product and its ability to track light objects to a high degree of accuracy. Errors using this system were well within the error budget specifications. Piston control was found to be successful using very simple algorithms. The algorithms when used with very noisy sensors, were found to be able to control the piston movement to within a very small distance.

Several LCSS spin-off commercial products were further developed and started during the Phase II effort. Opti-Trak 100, the most successful of these products, showed sales of several units during the Phase II effort that would have been near impossible without the added LCSS research. INSPECT, another commercialized product, has also been a success due to the Phase II LCSS effort. INSPECT is currently being further developed as part of a contract with the Tennessee Valley Authority to be used for remote power line inspection.

The main LCSS concept has also seen great success in the commercialization area. Preliminary conversations with Rockwell International have been fruitful at jointly selling the LCSS concept to a national surveillance organization. NASA also showed interest in the LCSS concept and their requirements will be addressed in the near future.

The LCSS Phase II SBIR effort was a success. Each of the objectives were met as per the contract and several follow-on options, both commercial and government, have become available due to this effort. Commercialization, an important SBIR activity, has also been very successful.



## DISTRIBUTION LIST

AUL/LSE Bldg 1405 - 600 Chennault Circle Maxwell AFB, AL 36112-6424	1 cy
DTIC/OCP 8725 John J. Kingman Rd, Suite 0944 Ft Belvoir, VA 22060-6218	2 cys
AFSAA/SAI 1580 Air Force Pentagon Washington, DC 20330-1580	1 cy
PL/SUL Kirtland AFB, NM 87117-5776	2 cys
PL/HO Kirtland AFB, NM 87117-5776	1 cy
Official Record Copy PL/VTS/Capt Cobb Kirtland AFB, NM 87117-5776	2 cys
PL/VT Dr Wick Kirtland AFB, NM 87117-5776	1 cy